Rap1 promotes epithelial integrity and cell viability in a growing tissue

C. Luke Messer and Jocelyn A. McDonald*

Division of Biology, Kansas State University, Manhattan, KS 66506

*Correspondence: jmcdona@ksu.edu

Running Title: Rap1 promotes epithelial integrity and cell survival

Abstract

Having intact epithelial tissues is critical for embryonic development and adult homeostasis. How epithelia respond to damaging insults or tissue growth while still maintaining intercellular connections and barrier integrity during development is poorly understood. The conserved small GTPase Rap1 is critical for establishing cell polarity and regulating cadherin-catenin cell junctions. Here, we identified a new role for Rap1 in maintaining epithelial integrity and tissue shape during *Drosophila* oogenesis. Loss of Rap1 activity disrupted the follicle cell epithelium and the shape of egg chambers during a period of major growth. Rap1 was required for proper E-Cadherin localization in the anterior epithelium and for epithelial cell survival. Both Myo-II and the adherens junction-cytoskeletal linker protein α-Catenin were required for normal egg chamber shape but did not strongly affect cell viability. Blocking the apoptotic cascade failed to rescue the cell shape defects caused by Rap1 inhibition. One consequence of increased cell death caused by Rap1 inhibition was the preferential loss of the polar cells, which later in development led to fewer cells forming a properly migrating border cell cluster. Our results thus indicate dual roles for Rap1 in maintaining epithelia and cell survival in a growing tissue during development.

Introduction

Epithelia serve critical functions throughout the body's tissues and organs. For proper homeostasis, epithelia must remain a cohesive unit while being amenable to essential remodeling events. This allows critical epithelial functions such as forming a barrier to pathogens, absorption of nutrients, wound healing, and other important roles (Abramson and Anderson, 2017; Blanpain and Fuchs, 2009; Bröer, 2008; Guillot and Lecuit, 2013; Tai et al., 2019). During development, epithelial tissues undergo dramatic tissue rearrangements while staying intact, for example in convergent extension in *Drosophila* (Irvine and Wieschaus, 1994), ventral enclosure in *C. elegans* (Williams-Masson et al., 1997), and bottle cell invagination in *Xenopus* (Keller, 1981). Once formed, cells in epithelia must maintain polarized cell shapes, stay connected through cell-cell contacts, and survive insults imposed by the tissue environment. Epithelial tissues are challenged by cell turnover, cellular rearrangements, and apoptosis in response to normal tissue growth and homeostasis (Duszyc et al., 2017; Guillot and Lecuit, 2013). Because dysregulation of epithelia shape and cell survival can lead to diseases such as cancer, it is important to understand the mechanisms required for epithelial maintenance.

Here we report a requirement for the conserved small GTPase Rap1 in epithelial maintenance, where it contributes both to cell and tissue shape and to cell viability. The *Drosophila* ovary is an excellent model system to investigate how epithelial cells and tissues respond to challenges such as growth and shape changes during development. The ovary is made up of a series of continuously developing egg chambers. Each egg chamber consists of an inner population of germline derived cells enveloped in a continuous, polarized somatic cell epithelium made of follicle cells. Follicle cells continue to divide until stage 6, when mitosis ceases, resulting in a monolayer of ~650 cells. The follicle cells undergo a unique rotational migration that helps assemble a basement membrane layer . The basement membrane provides resistance to tissue growth and contributes to egg chamber shape (Duhart et al., 2017). The egg chamber starts out round but eventually grows and elongates to an ellipsoid shape starting in mid-oogenesis. During this process, the inner germline cells expand and press against the follicle cell layer, contributing to the characteristic ovoid shape of the egg. It is critical that the epithelium stays intact to allow successful oogenesis and proper development of a mature, fertilizable egg.

Rap1 plays key roles in epithelial morphogenesis during development, particularly in the establishment of tissue polarity and cell-cell adhesions. In *Drosophila*, Rap1 helps polarize

79 epithelial cells by positioning Bazooka/Par3 (Bonello et al., 2018; Choi et al., 2013) and
80 promotes proper cell-cell adhesion by regulating E-Cadherin-rich adherens junctions (Knox and
81 Brown, 2002). In human podocytes, as well as other cell types, Rap1 regulates integrin
82 mediated adhesion to the basement membrane (Potla et al., 2014). Rap1 also promotes
83 dynamic cell shape changes during development, including the elongation of cells at the leading
84 edge of the lateral epidermis during *Drosophila* dorsal closure (Boettner and Van Aelst, 2007;
85 Boettner et al., 2003).
86 Here we show that Rap1 GTPase maintains cell and epithelial shapes and promotes
87 follicle cell survival during oogenesis. Loss of Rap1 altered the shape of follicle cells and the
88 egg chamber itself. We find that Rap1 contributes to cell and tissue morphogenesis during mid-
89 oogenesis by ensuring successful actomyosin contractility through the α-Catenin/E-Cadherin
90 adherens junctions in epithelial cells. Notably, inhibition of Rap1 also induced abnormal
91 apoptosis of follicle cells. The pro-survival function of Rap1 was especially important in a
92 specialized pair of epithelial follicle cells, the polar cells, during mid-oogenesis. When Rap1 was
93 inhibited, polar cells failed to maintain Death-associated inhibitor of apoptosis 1 (DIAP1),
94 leading to loss of one or both polar cells. This subsequently led to fewer cells assembling into
95 the migratory border cell cluster. Together, our results reveal dual roles for Rap1 in cell and
96 epithelial morphogenesis and promoting cell viability within a developing tissue.

97 **Results**

98 **Rap1 GTPase is required for proper egg chamber and epithelial shapes in mid-oogenesis**

99 To better understand the role of Rap1 in epithelial maintenance, we first analyzed the
100 localization of Rap1 using a functional GFP-Rap1 fusion protein expressed under the control of
101 the endogenous *Rap1* promoter (Knox and Brown, 2002). Rap1 is expressed ubiquitously in all
102 cells of the ovary, with highest enrichment at the apical cell cortex of follicle cells, including the
103 polar cells (Fig. 1A). While Rap1 has known roles in the morphogenesis of diverse epithelia
104 (Kim et al., 2022; Knox and Brown, 2002; Wang et al., 2013), few studies have analyzed how
105 Rap1 maintains epithelia during tissue growth. To address this, we inhibited Rap1 activity in the
106 follicle cells using a validated dominant negative Rap1 construct, UAS-DN-Rap1^{N17} (DN-
107 Rap1^{N17}), whose expression causes phenotypes that strongly resemble loss of *Rap1* or Rap1
108 RNAi knockdown phenotypes in the embryo and ovary (Boettner et al., 2003; Perez-Vale et al.,
109 2022; Sawant et al., 2018). DN-Rap1^{N17} was driven by an epithelial-specific GAL4 driver, *c306*-
110 GAL4 (Fig. 1B). Expression of *c306*-GAL4 begins early during oogenesis in anterior and
111 posterior follicle cells, but the highest expression occurs at mid-oogenesis (~stages 4-8). These

112 stages coincide with a major egg chamber growth phase, that requires the follicular epithelium
113 to stretch and challenges epithelial cell cohesion (Balaji et al., 2019; Crest et al., 2017; Haigo
114 and Bilder, 2011; Spradling 1993).
115 The shape of egg chambers at stages 4-to-6 appeared to be normal in both control and
116 DN-Rap1^{N17} egg chambers (Fig. 1C-D). However, by stages 7-8, the tissue shape of DN-
117 Rap1^{N17}-expressing egg chambers was no longer normal, particularly at the anterior end (Fig.
118 1D). The anterior of DN-Rap1^{N17} egg chambers was wider and flatter compared to control (Fig.
119 1C-D). Closer inspection revealed altered anterior epithelial follicle cell shapes specifically in the
120 *c306*-GAL4 expression region (Fig. 1B, D). DN-Rap1^{N17} follicle cells appeared to be stretched,
121 rather than the expected cuboidal follicle cell shapes in control egg chambers at these stages
122 (Fig. 1E-F). We further quantified the observed differences in anterior egg chamber shape,
123 which we termed "local deformation". To do this, we measured the width of the anterior egg
124 chamber at 20% of the total egg chamber length from the anterior end (*see* Materials and
125 Methods). Control egg chambers retained a characteristic "wedge" shape in this anterior region
126 (mean of 37.49μm). DN-Rap1^{N17} inhibited egg chambers, however, were wider and more "cup"
127 shaped (mean of 47.37μm; Fig. 1G). These data together suggest that Rap1 promotes tissue
128 and epithelial cell shapes during mid-oogenesis.
129

130 **Rap1 promotes polar cell shape and apical E-Cadherin accumulation**

131 In addition to the overall distorted anterior follicular epithelial cell shapes in DN-Rap1^{N17} egg
132 chambers, we observed particularly misshapen anterior polar cells compared to control (Fig. 1E-
133 F; 2A-B"). Polar cells are a specialized pair of follicle cells found at each pole of the egg
134 chamber. Polar cells are one of the first specified follicle cells in the ovary and express unique
135 cell markers such as the adhesion protein Fasciclin III (Fas III) (Ruohola et al., 1991). Because
136 anterior egg chamber shape was most impacted by Rap1 inhibition, we focused on the anterior
137 polar cells. We asked when and how polar cell shape was altered by loss of Rap1 activity. To do
138 this, we quantified anterior polar cell shapes by defining their aspect ratio (AR). We measured
139 the width of each polar cell along their dorsoventral (DV) axis and divided by their length along
140 the anterior-posterior (AP) axis (Fig. 2C). Control polar cells at stages 4-6 were typically longer
141 along the AP axis than they were wide along the DV axis (AR=0.61; Fig. 2A, A', C). At stages 4-
142 6, DN-Rap1^{N17} polar cell shape resembled control (AR=0.65; Fig. 2B, B', C). Control polar cells
143 maintained their earlier ellipsoid shape at stages 7-8, although they lengthened slightly along
144 the AP axis (AR=0.56; Fig. 2A, A", C). In contrast, Rap1 inhibited polar cells at stages 7-8

145 frequently lost this elliptical shape and were now extended along the DV axis, with more
146 spherical shapes (AR=1.02; Fig. 2B, B", C). Rap1-inhibited egg chambers also had more
147 extreme cases of abnormal polar cell morphology, with either one polar cell that appeared to be
148 missing (Fig. S1A) or a distortion of the polar cell pair, such as pulling apart into "dumbbell" type
149 shapes (Fig. S1B).
150 The defective polar cell shapes combined with examples that appeared to split apart
151 prompted us to ask if polar cells in DN-Rap1^{N17} egg chambers were less adhesive. The
152 homophilic cell-cell adhesion protein E-Cadherin accumulates at high levels in polar cells
153 (Niewiadomska et al., 1999). E-Cadherin, as well as the associated cadherin-catenin complex
154 member β-Catenin, highly localizes to the apical side of polar cells, particularly in the region
155 where the polar cell pair is apically constricted (Niewiadomska et al., 1999; Peifer et al., 1993).
156 Therefore, we next investigated if DN-Rap1^{N17} egg chambers accumulated E-Cadherin normally
157 in polar cells (Fig. 3). We measured the apical E-Cadherin fluorescence intensity in stages 7-8
158 egg chambers along a line drawn starting over the anterior-most nurse cell ("1"; Fig. 3A', B') that
159 extended through the apical polar cell-polar cell interface to the lateral interface ("2"; Fig. 3A', B',
160 C). In control egg chambers, we observed a peak in fluorescence signal as the line passed
161 through the apical polar cell-polar cell interface (Fig. 3A-A", C, D). Strikingly, in DN-Rap1^{N17} egg
162 chambers the apical fluorescence enrichment is severely decreased and resembled the
163 intensity values for the portion of the line that extended along the lateral interface (Fig. 3B-B", C,
164 D). These results indicated that Rap1 controls the localized enrichment of E-Cadherin to the
165 apical interface between polar cells, which in turn may promote the normal shape of the polar
166 cell pair.
167 Non-muscle myosin II (Myo-II), as visualized with a functionally-tagged regulatory light
168 chain, Spaghetti Squash-GFP, Sqh::GFP (Royou et al., 2004), is enriched across the entire
169 apical surface of the anterior polar cell pair as well as other follicle cells (Fig. S2A-A''). However,
170 we did not observe any obvious differences in the accumulation of Sqh:GFP at the apical
171 surface of DN-Rap1^{N17} polar cells (Fig. S2B-B"). To confirm this, we quantified Sqh::GFP
172 accumulation by drawing a line across the apical surface of the polar cell pair. We then plotted
173 profiles of the fluorescent intensity values from at least 8 polar cell pairs per genotype. These
174 data indicated no major differences in the Myo-II levels or patterns between control and DN-
175 Rap1^{N17} polar cells (Fig. S2C). Together, our results indicate that Rap1 is dispensable for
176 accumulation of Myo-II but is required for E-Cadherin apical enrichment in polar cells at mid-
177 oogenesis.
178

179 **Myo-II and α-Catenin are required for egg chamber morphogenesis**
180 Actomyosin contractility and adhesion both contribute to the shape and integrity of various
181 tissues and organs during development (Harris and Tepass, 2010; Munjal and Lecuit, 2014).
182 Therefore, we wanted to assess whether actomyosin contractility was required for local tissue
183 morphogenesis similar to what we observed for Rap1 (Fig. 4A-E). We targeted the Myo-II
184 regulatory light chain with RNAi-mediated knockdown (Sqh RNAi) and measured local (anterior)
185 tissue deformation. Myo-II deficient staged 7-8 egg chambers resembled what we observed in
186 DN-Rap1^{N17} inhibited egg chambers; the anterior tissue shape was wide and flat (compare Fig.
187 4B, E to Fig. 1F, G). These results were unexpected given that Rap1 inhibition did not affect
188 apical Myo-II accumulation, at least in polar cells. Therefore, we reasoned that Rap1 may
189 couple actomyosin contractility to the adherens junctions in the anterior epithelium, as has been
190 described in other tissues (Sawyer et al., 2009).
191 To test this hypothesis, we next performed RNAi knockdown of E-Cadherin and α-
192 Catenin, members of the adherens junction complex. Surprisingly, E-Cadherin had no effect on
193 egg chamber morphogenesis. Anterior width measurements were no different in E-Cadherin
194 deficient egg chambers when compared to GFP RNAi controls (Fig. 4A, C, E). However, N-
195 cadherin is expressed during these stages and has been shown to undergo compensatory
196 upregulation due to loss of E-Cadherin (Loyer et al., 2015). Thus, we next knocked down α-
197 Catenin (α-Cat), the linker protein that connects cadherin complex members to the cellular F-
198 actin cytoskeleton (Wang et al., 2022; Yonemura et al., 2010). Indeed, downregulation of α-
199 Catenin by RNAi resulted in a wider anterior egg chamber, resembling the tissue shape defects
200 observed with Sqh RNAi and inhibition of Rap1 activity (Fig. 4B, D-E; Fig. 1F-G). Thus,
201 adhesion and actomyosin are required to maintain tissue shapes at mid-oogenesis stages.
202 We next examined the shape of epithelial follicle cells at the anterior end of the egg
203 chamber when Myo-II or α-Catenin were knocked down by RNAi (Fig. 4F-I'). Close inspection
204 revealed altered individual cell shapes resembling DN-Rap1^{N17} egg chambers only for α-Catenin
205 RNAi (Fig. 4 H-I') but not Sqh RNAi (Fig. 4G, G'). Notably, we observed a mix of "stretched" or
206 "flattened" follicle cells in α-Catenin RNAi egg chambers along the lateral sides of the egg
207 chamber that looked like the cells in the anterior region of DN-Rap1^{N17} egg chambers (Fig. 4H-I';
208 compare to Fig. 1F). In the most-affected α-Catenin RNAi egg chambers (Fig. 4I, I'), clumping of
209 cells was observed at the most anterior end and closely resembled the cell shapes reported for
210 *α-Catenin* null mutant follicle cells (Sarpal et al., 2012). The similarities in the tissue and
211 epithelial cell shape phenotypes caused by loss of α-Catenin and Rap1 activity suggested that

212 Rap1 modulates α-Catenin-containing adherens junctions as was observed during dorsal fold
213 formation in the *Drosophila* embryo (Wang et al., 2013).

214 **Rap1 promotes the viability of epithelial follicle cells during oogenesis**

215 Our analysis of DN-Rap1^{N17} egg chambers at stages 7-8 revealed not only cases of extremely
216 distorted polar cells, but also examples where one polar cell was missing from the required pair
217 (Fig. S1A). These data suggested that Rap1 contributes to cell survival. To test this idea, we
218 first analyzed a marker of apoptosis during oogenesis in control and Rap1 mutant ovaries. We
219 stained egg chambers for antibodies to cleaved death caspase-1 (cDcp-1), which recognizes
220 both *Drosophila* effector caspases, Death caspase-1 (Dcp-1) and Death related ICE-like
221 caspase (Drice) (Li et al., 2019). During early oogenesis, excess polar cells ("supernumerary"
222 polar cells) and excess stalk cells form but are eliminated by apoptosis during stages 3-6,
223 whereas in healthy ovarioles other follicle cells do not undergo cell death (Borensztejn et al.,
224 2013; Borensztejn et al., 2018; Khammari et al., 2011; Lebo and McCall, 2021; cDCp-1+ cells;
225 Fig. 5A). However, in DN-Rap1^{N17} ovarioles, in addition to the normal pattern of early polar cell
226 and stalk cell apoptosis, we observed additional caspase activity in follicle cells during stages 2
227 through 8 of oogenesis (cDCp-1+ cells; Fig. 5B). We quantified the number of cDcp-1 cells in
228 control and DN-Rap1^{N17} ovarioles and saw a significant increase in apoptotic cells only when
229 Rap1 activity was inhibited (Fig. 5C). Activation of Rap1, through expression of constitutively
230 active CA-Rap1^{V12} did not decrease apoptotic cells during any stage of oogenesis (Fig. 5C).
231 These data suggest that Rap1 is required for follicle cell survival during oogenesis but is not
232 sufficient to block normal developmental apoptosis.

233 Because Rap1 promotes both follicle cell survival and epithelial and tissue
234 morphogenesis during oogenesis, we next asked if Myo-II or α-Catenin were also similarly
235 required for follicle cell viability. We analyzed cell death during oogenesis using cDcp-1 in Sqh
236 RNAi, α-Catenin RNAi, and matched control (GFP RNAi) ovarioles. We observed minimal cell
237 death in Sqh RNAi and GFP RNAi controls (Fig. 5D, E, G). However, there was a significant
238 increase in cDcp-1 positive cells for α-Catenin RNAi ovarioles (Fig. 5F, G). These results
239 suggest that while both Myo-II and α-Catenin regulate egg chamber morphogenesis, only α-
240 Catenin is required for viability of the follicle cells. Notably, although α-Catenin RNAi results in
241 an increase in cDcp-1 positive cells, fewer cells per ovariole were cDcp-1 positive than when
242 Rap1 was inhibited (2.6 cDcp-1-positive cells for α-Catenin RNAi, Fig. 5G, compared to 8.8
243 cDcp-1-positive cells per ovariole for DN-Rap1^{N17}, Fig. 5C). These findings suggest that cell

244 adhesion via α-Catenin is required for cell viability, though Rap1 may have a greater role in
245 promoting cell survival.
246
247 **Rap1 promotes polar cell survival by suppressing apoptosis, but polar cell shape defects**
248 **are not apoptosis-dependent**
249 As described above, loss of Rap1 activity causes death of follicle cells and loss of polar cells
250 (Fig. 5B-C; Fig. S1A), in addition to defects in polar cell shape (Fig. 2B-C; Fig. S1B). Therefore,
251 we wanted to determine if Rap1 was required to manage elimination of supernumerary polar
252 cells that form at each pole of early egg chambers (Besse and Pret, 2003; Borensztejn et al.,
253 2013; Khammari et al., 2011). Removal of the extra polar cells by apoptosis ensures that only
254 two "mature" polar cells remain at anterior and posterior egg chamber poles by stages 5/6
255 (Besse and Pret, 2003; Borensztejn et al., 2013; Khammari et al., 2011). One possibility for the
256 absence of polar cells in later staged DN-Rap1^{N17} egg chambers could be a requirement for
257 Rap1 in early polar cell development and elimination. Alternatively, Rap1 could promote the
258 survival of mature polar cells later in oogenesis after these cells are specified.
259 We examined anterior and posterior polar cells in egg chambers from stages 3-10 of
260 oogenesis using Eyes Absent (Eya) and FasIII (Fig. S3A). Eya suppresses polar cell fate and is
261 present in all follicle cells except polar cells (Bai and Montell, 2002) and FasIII specifically marks
262 the polar cell pair (Ruohola et al., 1991). We observed similar numbers of supernumerary polar
263 cells at early stages of development (e.g., stages 3-4 and stages 5-6) in control and DN-Rap1^{N17}
264 (Fig. S3A). Using CA-Rap1^{V12}, we next asked if increased Rap1 activity resulted in extra polar
265 cells being maintained until maturity. At each stage examined, we observed similar numbers of
266 polar cells for CA-Rap1^{V12} and controls (Fig. S3A). Moreover, in all genotypes, in agreement
267 with other studies, there was an overall decrease in the number of polar cells as oogenesis
268 progressed (Fig. S3A; Borensztejn et al., 2013; Khammari et al., 2011).
269 Since early polar cell development appeared normal in Rap1-deficient egg chambers,
270 we next asked if Rap1 regulated the survival of mature polar cells later in oogenesis. We
271 tracked polar cell-specific accumulation of cDcp-1. Control "mature" polar cells at stages 7-8
272 rarely died (Fig. 6A-A";1 out of 66 egg chambers). In contrast, we observed an increased
273 frequency in the accumulation of cDcp-1 in staged 7-8 DN-Rap1^{N17} polar cells, well after the
274 conclusion of normal developmental apoptosis (Fig. 6B-B"; 7 out of 61 egg chambers). These
275 polar cells were frequently pyknotic as visualized by DAPI staining (Fig. 6B'). These data
276 together indicate that Rap1 promotes the survival of both follicle cells and mature polar cells
277 during oogenesis.

278 To further characterize this increase in polar cell death when Rap1 was inhibited, we
279 next examined the apoptotic cascade. Death-associated inhibitor of apoptosis 1 (DIAP1) blocks
280 caspase activity and thus prevents cells from undergoing apoptosis (Hay et al., 1995; Yan et al.,
281 2004). DIAP1 specifically accumulates in the two mature polar cells and promotes their survival,
282 whereas DIAP1 is downregulated in the supernumerary polar cells leading to their
283 developmental apoptosis (Borensztejn et al., 2013; Khammari et al., 2011). We reasoned that a
284 decrease in DIAP1 might precede the death of mature polar cells observed in DN-Rap1^{N17} egg
285 chambers. Therefore, we analyzed DIAP1 accumulation in polar cells relative to their most
286 adjacent follicle cell neighbors at both stages 4 to 6 and at stages 7 to 8. At the earlier stages
287 (stages 4-6), we observed normal accumulation of DIAP1 in 13 out of 14 control polar cells (Fig.
288 6C-C"). However, DIAP1 accumulated in only 6 out of 23 DN-Rap1^{N17} polar cells (Fig. 6E-E").
289 Similarly, at later stages, DIAP1 accumulation was lower in DN-Rap1^{N17} inhibited polar cells,
290 with only 8 out of 19 egg chambers having normal DIAP1 accumulation (Fig. 6F-F"), compared
291 to 10 out of 14 for control egg chambers (Fig. 6D-D"). Interestingly, DIAP1 levels were altered at
292 a greater frequency in DN-Rap1^{N17} egg chambers (Fig. 6E-F") than the observed frequency of
293 polar cell death (Fig. 6B"). One possibility is that not all cells that lose DIAP1 accumulation
294 undergo cell death. Alternatively, the threshold for DIAP1 protein depletion may need to be
295 relatively severe for apoptosis to occur. Taken together, our results favor a role for Rap1 in
296 suppressing the apoptotic cascade through regulating the levels of DIAP1 in mature polar cells.
297 We next asked if the polar cell morphology defects caused by loss of Rap1 activity were
298 due to apoptosis. To test this, we asked if blocking the apoptotic cascade could rescue polar cell
299 shape defects caused by loss of Rap1 activity (Fig. S3B-D). We performed polar cell aspect
300 ratio measurements in egg chambers that co-expressed DN-Rap1^{N17} with either a LacZ control
301 or with the apoptosis inhibitor, baculoviral p35 (Clem et al., 1991; Hay et al., 1994). We found
302 that co-expression of p35 along with DN-Rap1^{N17} failed to rescue the polar cell aspect ratio
303 defects compared to co-expression with LacZ (Fig. S3B-D). There was no statistical difference
304 in the aspect ratios of DN-Rap1^{N17} polar cells either co-expressing the LacZ control or p35
305 (AR=0.84, DN-Rap1^{N17} + LacZ; AR=0.85, DN-Rap1^{N17} + p35; Fig. S3D). These results provide
306 further evidence that Rap1 likely controls polar cell morphogenesis independently of its function
307 in promoting cell survival.
308

309 **Rap1 requirement for polar cell survival supports formation of border cell clusters with**
310 **optimal cell numbers**

311 The role for Rap1 in promoting polar cell survival prompted us to ask what the developmental
312 consequences were later in oogenesis. During late stage 8, the anterior pair of polar cells
313 specifies which follicle cell neighbors become the migratory border cells through the secretion of
314 the JAK/STAT ligand Unpaired (Beccari et al., 2002; Silver and Montell, 2001). Between 4-8
315 follicle cells activate high levels of JAK/STAT and subsequently surround the polar cells to
316 produce a border cell cluster with a total of 6 to 10 cells (Silver and Montell, 2001). Having an
317 optimal number of cells helps the border cell cluster efficiently reach the oocyte at the correct
318 time (Cai et al., 2016; Starz-Gaiano et al., 2008; Stonko et al., 2015)

319 Because inhibition of Rap1 caused a frequent loss of mature polar cells, we determined
320 how this impacted the size of the migratory border cell cluster. We reasoned that losing a polar
321 cell might decrease the number of cells found in border cell clusters. We quantified the total
322 number of cells found within control (UAS-LacZ) versus Rap1-deficient (UAS-Rap1^{N17} or UAS-
323 Rap1 RNAi) border cell clusters (Fig. 7 A-C). When Rap1 was inhibited using with DN-Rap1^{N17}
324 driven by *c306*-GAL4, we found a strong reduction in the average number of cells per cluster
325 compared to control (Fig. 7A', B'; average of 6.1 cells in control compared to 4.6 cells in DN-
326 Rap1^{N17}). *c306*-GAL4-driven *Rap1* RNAi also reduced the number of cells per cluster to an
327 average of 5.2 cells compared to 6.1 cells in *mCherry* RNAi controls (Fig. 7C). We analyzed the
328 number of cells in border cell clusters using a different GAL4, *slbo*-GAL4, which is expressed
329 later than *c306*-GAL4 and in a more restricted pattern (Fig. S4A). The overall number of cells in
330 *slbo*-GAL4 control egg chambers is higher than that observed for *c306*-GAL4 controls (average
331 of 8.2 cells; Fig. S4B, B', D). Nonetheless, we observed a significant reduction in the number of
332 DN-Rap1^{N17} cells within the border cell cluster (Fig. S4C-D; average 6.7 cells). Thus, Rap1 is
333 required for migrating border cell clusters to have an optimal number of cells.

334 We next asked if the observed reduction in cell numbers within the border cell cluster
335 was due to Rap1 function in border cell specification or in the recruitment of cells due to cell
336 survival. We examined anterior follicle cells at stage 8 for a reporter of JAK/STAT activity,
337 10XSTAT::GFP (Bach et al., 2007). These cells are fated to become the migratory border cells
338 (Beccari et al., 2002; Silver and Montell, 2001). When both polar cells were present, we did not
339 detect changes in either the pattern of 10XSTAT:GFP or the levels of nuclear STAT, and hence
340 activity, in the three follicle cells immediately adjacent to the polar cells at stages 7-8 in DN-
341 Rap1^{N17} compared to control (Fig. S5A-C). These results suggest that border cell fate
342 specification at stage 8 of oogenesis is normal under conditions when both polar cells are

343 present and does not rely on Rap1 activity. However, we cannot rule out a subtle decrease in
344 the JAK/STAT activity gradient when only one polar cell survives to stage 8 in DN-Rap1^{N17} egg
345 chambers.
346 Finally, we determined if the smaller number of cells per border cell cluster was due to
347 the increased apoptotic activity observed upon Rap1 inhibition. We co-expressed DN-Rap1^{N17}
348 with either a UAS-LacZ control or the apoptosis inhibitor p35 (Fig. 7D-F). We quantified the
349 number of cells per cluster at stages 9 and 10, when border cell clusters have already formed
350 and have either begun to migrate or finished their migration. Border cell clusters that co-
351 expressed DN-Rap1^{N17} and LacZ had an average of 4.8 cells per cluster, resembling the
352 phenotypes observed when expressing DN-Rap1^{N17} alone (Fig. 7D, D', F compared to Fig. 7C).
353 In contrast, border cell clusters co-expressing DN-Rap1^{N17} and p35 had an average of 6.4 cells
354 per cluster (Fig. 7E-F), matching control border cell clusters (Fig. 7A, A', C). Thus, the observed
355 smaller border cell clusters caused by loss of Rap1 activity is likely due to apoptotic cell death of
356 mature polar cells just prior to recruitment of border cells. Together, these data support a model
357 in which Rap1 promotes mature polar cell survival by preventing apoptosis through upregulation
358 of DIAP1, thus promoting an optimal number of cells being recruited to form the migrating
359 border cell cluster.
360
361 **Discussion**
362 A key challenge is to understand how epithelia and constituent cells survive and maintain shape
363 in response to the changes in tissue shape and size during normal development. Here we
364 focused on understanding how the small GTPase Rap1 maintains cell and tissue shapes during
365 *Drosophila* egg chamber growth. Prior work has shown requirements for Rap1 in epithelial
366 morphogenesis (Asha et al., 1999; Boettner and Van Aelst, 2007; Choi et al., 2013; Bonello et
367 al., 2018), but whether and how Rap1 maintains epithelia during tissue growth and homeostasis
368 was unclear. Here we used a model of developmental tissue growth in the *Drosophila* ovary to
369 interrogate the function of Rap1. We found that Rap1 promotes epithelial follicle cell shape,
370 polar cell shape, and local tissue shapes during a period of major egg chamber growth. We
371 propose that this function of Rap1 in maintenance of epithelial integrity is through regulation of
372 dynamic linkages between adherens junctions and the contractile actomyosin cytoskeleton. Our
373 experiments revealed an unexpected and new role for Rap1 in regulating cell survival,
374 especially of the mature polar cells, which leads to the assembly of a migratory border cell
375 cluster with the optimal number of cells.
376

377 **Rap1 maintains cell and tissue shapes by modulating adherens junction-cytoskeleton**
378 **linkages during tissue growth**
379 Here we report that Rap1 is required to maintain polar cell and follicle cell shapes and proper
380 tissue shapes of the anterior follicular epithelium during egg chamber elongation. Our
381 quantitative analyses of individual cell shapes and local tissue deformation demonstrated that
382 Rap1 maintained tissue and epithelial morphology. Moreover, Rap1-deficient polar cell shapes
383 were highly affected. Most of these phenotypes were at stages 7-8, a period of dramatic egg
384 chamber growth (Crest et al., 2017). Previous work using *Rap1* null flies that were rescued to
385 viable adults by expression of heat shock-driven Rap1 revealed egg chambers that degenerated
386 and had distorted follicle cell shapes (Asha et al., 1999). Notably, these phenotypes seemed to
387 be more severe during mid-to-late stages of oogenesis, stages that overlap with egg chamber
388 elongation, thus supporting a role for Rap1 in tissue maintenance. We obtained similar, albeit
389 less severe egg chamber defects, by specifically expressing DN-Rap1^{N17} in follicle cells. These
390 results indicate a requirement of Rap1 in tissue shape maintenance.
391 How does Rap1 contribute to cell and tissue shape maintenance within the follicular
392 epithelium during tissue expansion? Rap1 regulates early Bazooka/Par3 localization and
393 adherens junction positioning during *Drosophila* embryogenesis (Bonello et al., 2018). *Rap1*
394 mutant embryos fail to localize spot adherens junctions properly during cellularization and
395 complete embryogenesis with fragmented cuticles suggesting a loss of tissue integrity (Choi et
396 al., 2013). Similarly, Rap family proteins are required for adherens junctions and tight junction
397 formation in MDCK cells (Sasaki et al., 2020). Our results showed that Rap1 is required
398 specifically for the enrichment of E-Cadherin at the apical side of polar cells, which we propose
399 helps promote proper polar cell shapes. We also observed stretching of the anterior epithelial
400 follicle cells, which may indicate altered adhesion in these cells. Although E-cadherin appeared
401 to be localized to apical puncta between follicle cells consistent with the formation of adherens
402 junctions, these junctions may not be completely normal thus contributing to the stretched
403 epithelial shapes. We thus propose that Rap1 maintains (or helps assemble) the proper
404 positioning of the apical adherens junction, at least in polar cells. Further work will be needed to
405 determine if and how Rap1 mechanistically maintains adherens junctions in the follicle cells.
406 The functions of adherens junctions to maintain cell-to-cell contacts within an epithelium
407 are also coupled to actomyosin contractility, which can drive cell shape changes. Rap1 and its
408 effector Canoe (Cno) regulate actomyosin contractility in apically constricting mesodermal cells
409 during *Drosophila* ventral furrow invagination (Sawyer et al., 2009; Spahn et al., 2012).
410 Similarly, Rap1 is required for Shroom dependent apical constriction in *Xenopus* (Haigo et al.,

411 2003). These studies led us to ask if, in addition to its role in positioning adherens junctions
412 during egg chamber elongation, Rap1 was responsible for proper actomyosin contractility. We
413 found that Myo-II was required for proper tissue shape during egg chamber elongation, but
414 surprisingly Rap1 was dispensable for Myo-II localization in polar cells. Taken together with the
415 stretched individual cell shapes and deformed egg chambers observed for α-Catenin RNAi,
416 these data support our model that Rap1 maintains the strength of adherens junction-actin
417 linkages as was reported for the known Rap1 effector Cno (Sawyer et al., 2009).
418 We found that Rap1 regulates egg chamber shape during a period of major tissue
419 growth. The inherent on-off activity states of GTPases like Rap1 make them particularly useful
420 for dynamic processes that require discrete bursts of activity in response to cellular or tissue
421 level cues (Gloerich and Bos, 2011). In apical constriction, for example, myosin pulsatility is
422 coupled to progressive tightening of the apical domain (Martin and Goldstein, 2014; Martin et
423 al., 2009). The transient nature of pulsatile myosin may require a fast-acting molecular switch
424 that can be activated and inactivated quickly to couple motor behaviors to changes at the cell
425 cortex. While we did not observe Myo-II localization defects when Rap1 was inhibited, the
426 requirement for α-Catenin indicates that linkage to the actomyosin cytoskeleton is critical for
427 epithelial cell and tissue shapes. Atypical Protein Kinase C (aPKC) promotes an optimal level of
428 actomyosin to maintain an intact and organized follicle cell epithelium (Osswald et al., 2022).
429 Indeed, acute loss of aPKC causes the follicle cell layer to apically constrict and rupture, due to
430 growth of the egg chamber. While the effects caused by loss of Rap1 activity did not cause the
431 epithelium to rupture, the tissue instead locally deformed. The basement membrane becomes
432 thinner at the anterior and posterior ends during tissue elongation, allowing further growth along
433 the anterior-posterior axis (Balaji et al., 2019; Crest et al., 2017). We suggest that loss of Rap1,
434 in conjunction with a permissive region of the basement membrane, allows the tissue to widen
435 in response to egg chamber growth . Thus, we propose that Rap1, through apical enrichment of
436 adherens junction proteins, reinforces strong epithelial connections and resistance to growth of
437 the germline.
438 The signal relay mechanisms that act upstream to regulate the various Rap1 activities in
439 the follicle cell epithelium are unknown. Nor is it known which Rap1 effectors mediate the direct
440 control of adherens junction-actomyosin linkages in this context. The GTPase activating protein
441 Rapgap1 acts as one regulatory layer controlling Rap1 α-Catenin modulation in regulating
442 dorsal fold morphogenesis and is expressed in the ovary (Wang et al., 2013; Sawant et al.,
443 2018). *Drosophila* has several known guanine nucleotide exchange factors (GEFs), including
444 PDZ-GEF (also known as Dizzy), C3G, and Epac. Whether one or more GEFs have differential

445 functions during these stages of oogenesis, and in cell survival, remains to be tested. A well-
446 known Rap1 effector, Cno, acts as a key signal relay mechanism downstream of Rap1. For
447 example Cno mediates Rap1 functions in *Drosophila* morphogenesis including mesoderm
448 invagination, head involution, and dorsal closure through modular biochemical functions (Perez-
449 Vale et al., 2021; Sawyer et al., 2009). Whether these or other upstream and downstream
450 regulators mediate Rap1 functions in epithelial tissue maintenance and cell survival remain to
451 be determined.
452
453 **Rap1 promotes follicle cell and polar cell survival during oogenesis**
454 We found that Rap1 maintains epithelial cell viability during oogenesis. One possibility is that
455 the role for Rap1 in adherens junction protein localization is coupled to cell survival. Cell-cell
456 contacts are essential for cell viability in certain contexts (Guillot and Lecuit, 2013). We found
457 that the adherens junction-cytoskeleton linker protein α-Catenin not only supported proper
458 epithelial and tissue shapes, but also promoted cell survival during oogenesis. Thus, cell-cell
459 adhesions may be coupled to cell viability during tissue growth during oogenesis. Indeed, this
460 period of dramatic tissue growth places extra strain on the epithelial follicle cells (Osswald et al.,
461 2022), which could result in fewer cells surviving. Another major role for Rap1 was in promoting
462 survival of the mature polar cells. The consequence of fewer polar cells surviving was a smaller
463 border cell cluster, which is critical for optimal migration speed and ability to reach their final
464 position at the oocyte (Cai et al., 2016; Stonko et al., 2015). Thus, Rap1's role in promoting cell
465 viability is critical for normal oogenesis.
466 We do not yet have a clear understanding of the mechanism by which Rap1 promotes
467 cell survival and suppresses apoptosis. Our results suggest that Rap1 may have independent
468 functions in cell survival other than (or in addition to) regulation of adherens junction proteins.
469 Although knocking down α-Catenin resulted in apoptotic cells, the phenotype was overall much
470 milder than that observed with Rap1 inhibition. Normally, DIAP1 must be maintained in the two
471 mature polar cells to prevent their apoptosis (Borensztejn et al., 2013; Khammari et al., 2011).
472 We observed a decrease in DIAP1 accumulation in the mature polar cells upon Rap1 inhibition,
473 which is unlikely to be directly associated with defects in cell-cell adhesion. During stages 7 to 8,
474 the overall levels of DIAP1 undergo a global reduction, which serves as a checkpoint
475 mechanism to terminate unhealthy egg chambers rather than commit additional nutritional and
476 energy resources (Baum et al., 2007). Rap1 promotes levels of DIAP1 before and during these
477 stages, thus protecting the mature polar cells and likely other follicle cells from undergoing
478 abnormal cell death. It remains to be tested whether Rap1 generally maintains cell survival of

479 follicle cells by more directly fine tuning DIAP1 levels at the molecular level, or if the regulation
480 of DIAP1 by Rap1 is indirect, for example due to disruption of epithelial integrity when Rap1 is
481 inhibited. It is also unclear how cellular mechanics function together with transcription of DIAP1
482 to promote cell survival during tissue growth of the ovary. Further work will also be needed to
483 determine if the function for Rap1 in cell survival and maintenance of epithelial shapes in
484 growing tissues is conserved in other developing tissues and organs.
485
486
487 **MATERIALS AND METHODS**
488
489 ***Drosophila* genetics**
490 All fly stocks used in this study are listed in Table 1 and the complete genotypes for each
491 experiment can be found in Table 2. Crosses were typically set up and maintained at 25˚C. In
492 cases where transgene expression impacted organism viability, the crosses were set up and
493 maintained at 18˚C. The tub-GAL80ts ('tsGAL80') transgene (McGuire et al., 2004) was present
494 in the genetic background of many crosses in this study to repress GAL4 expression during
495 other stages of development. Flies were shifted to 29˚C for 12-72 hours prior to dissection to
496 ensure optimal GAL4 expression and repression of tsGAL80, unless otherwise noted.
497
498 **Immunostaining**
499 Antibodies, sources, and dilutions used are listed in Table 3. Fly ovaries from 2- to 8-day old
500 females were dissected in Schneider's *Drosophila* Medium (Thermo Fisher Scientific, Waltham,
501 MA, USA) supplemented with 10% fetal bovine serum (Seradigm FBS; VWR, Radnor, PA,
502 USA). Ovaries were either kept whole or dissected further into ovarioles and fixed for 10 mins
503 using 16% methanol-free formaldehyde (Polysciences, Inc., Warrington, PA, USA) diluted to a
504 final concentration of 4% in 1X Phosphate Buffered Saline (PBS). Following fixation, tissues
505 were washed ≥4x with 'NP40 block' (50 mM Tris-HCL, pH 7.4, 150mM NaCl, 0.5% NP40,
506 5mg/ml bovine serum albumin [BSA]) and rocked in the solution for ≥30 mins prior to antibody
507 incubation. Primary and secondary antibody incubation as well as all other subsequent wash
508 steps were also performed in NP40 block. Dissected and stained ovarioles and egg chambers
509 were mounted on slides with Aqua-PolyMount (Polysciences, Inc.) media and allowed to harden
510 prior to imaging.
511
512 **Microscopy**

513 Images of fixed egg chambers were acquired on a Zeiss LSM 880 confocal laser scanning
514 microscope (KSU College of Veterinary Medicine Confocal Core) using either a 20 X 0.75
515 numerical aperture (NA) or a 40 X 1.3 NA oil-immersion objective controlled by Zeiss Zen 14
516 software.
517
518 **Image Processing and Data Analysis**
519 Measurements were performed using FIJI (Schindelin et al., 2012). Egg chamber local
520 deformation measurements were determined by measuring the width between the apical follicle
521 cell surfaces at 20% of the anterior-posterior (A-P) length of the egg chamber (the very anterior
522 tip is 0% of the A-P length). The polar cell aspect ratio was measured by analyzing Z-stacks
523 taken of egg chambers stained with FasIII (to identify polar cells), E-Cadherin, and DAPI; the
524 length and width was measured at the widest point of each polar cell. The aspect ratio was then
525 calculated by dividing the width by length.
526 E-Cadherin accumulation in polar cells (identified by FasIII) was measured by analyzing
527 Z-stacks acquired of egg chambers stained for E-Cadherin, FasIII, and DAPI. A 7μm line was
528 drawn to quantify pixel intensity, starting within the germline (an adjacent nurse cell), extending
529 through the apical polar cell-polar cell contact, then continuing along the lateral interface (see
530 line in Fig. 3A' and 3B'). Only images in which both polar cells could be viewed in the same Z-
531 slice were used for quantitation. The "Plot Profile" function in FIJI was used to obtain a list of
532 pixel intensity values corresponding to points along this line. These values were normalized to
533 the highest pixel intensity measured in the experiment and plotted. Staining and imaging
534 conditions were kept consistent between samples.
535 Dying cells during oogenesis were quantified by scanning through dissected whole
536 ovarioles stained and imaged for cDcp-1, DAPI, and FasIII. Nuclei positive for caspase activity
537 (cDcp-1-expressing nuclei) from stages 2 through 8 were quantified. Death of mature polar was
538 scored by analyzing cDcp-1 expressing nuclei specifically in stage 7-8 egg chambers. DIAP1
539 accumulation in polar cells was assessed by acquiring Z-stacks through the polar cells in stages
540 4-6 and stages 7-8 egg chambers and analyzing qualitative reduction in the DIAP1 signal
541 compared to adjacent cells. Polar cells were identified using a GFP protein trap in FasIII.
542 Quantification of the number of cells per border cell cluster were measured by acquiring
543 Z-stacks through border cell clusters visualized using the nuclear envelope marker Lamin (also
544 known as Lamin Dm_0) and DAPI. Whenever possible, E-Cadherin was used to determine the
545 boundaries of fully delaminated border cell clusters. Z-stacks encompassing the entire cluster

546 including both border cells and polar cells were acquired and nuclei were manually counted
547 using the Lamin signal.
548 Apical Myo-II accumulation was quantified by acquiring Z-stacks of stage 7-8 egg
549 chambers expressing a fluorescent Myo-II reporter, Sqh::GFP, and co-stained for E-Cadherin
550 and DAPI. A 2μm line was drawn at the apical surface of polar cells (identified by enrichment of
551 E-Cadherin) and the "Plot Profile" function in FIJI was used to obtain a list of intensity values for
552 each line. The intensity values were normalized to the highest pixel intensity measured in the
553 experiment and plotted. Samples of inferior staining quality were eliminated from analysis.
554 Staining and imaging conditions were kept consistent between samples.
555 Supernumerary polar cell load during oogenesis was scored by scanning through whole
556 ovarioles and counting the number of polar cells present at each pole using FasIII and Eya as
557 markers for polar cell fate. Nuclear STAT intensity at stages 7-8 was quantified by measuring
558 10XSTAT::GFP reporter intensity by drawing lines across three nuclei on either side of polar
559 cells The mean GFP intensity of each line was normalized to the mean DAPI signal for each
560 nuclear measurement. All measurements were then normalized to the highest relative GFP
561 intensity value measured in the experiment.
562
563 **Figures, graphs, and statistics**
564 Images were processed in FIJI and figures were assembled using Affinity Photo (Serif,
565 Nottingham, United Kingdom). Illustrations were designed in Affinity Photo. Graphs and
566 statistical tests were performed using GraphPad Prism 7 or Prism 9 (GraphPad Software, San
567 Diego, CA, USA). All statistical tests and significance levels are listed in the figure legends for
568 the figures in which they appear and in Table 4.
569
570 **Acknowledgements**
571 We would like to thank Denise Montell, Michelle Starz-Gaiano, Nick Brown, and Hyung Don
572 Ryoo, the Vienna *Drosophila* Resource Center (VDRC), the Bloomington *Drosophila* Stock
573 Center (BDSC), and the Developmental Studies Hybridoma Bank (DSHB) at the University of
574 Iowa for fly protocols, fly stocks, and antibodies. We also thank Gibson Hoefgen and Manuel
575 Garcia for general project assistance and maintenance of *Drosophila* strains and Emily
576 Burghardt, Rehan Khan, and Yujun Chen for helpful comments on the manuscript. We
577 acknowledge the Confocal Core, funded by the Kansas State University (KSU) College of
578 Veterinary Medicine, which provided use of the Zeiss LSM 880 confocal microscope. We thank
579 the KSU Statistics Consulting Laboratory for statistics advice. This work was supported by the

National Science Foundation (NSF 2027617) to J.A.M. and a KSU Johnson Cancer Research Center Graduate Student Summer Stipend Award to C.L.M. and J.A.M. The authors declare no competing financial interests.

Author Contributions

C. Luke Messer: Conceptualization, Formal analysis, Validation, Investigation, Visualization, Methodology, Writing - Original Draft, Writing - Review & Editing; Jocelyn A. McDonald: Conceptualization, Supervision, Funding acquisition, Methodology, Writing - Original Draft, Writing - Review & Editing.

590
591 **References**
592

593 **Abramson, J. and Anderson, G.** (2017). Thymic Epithelial Cells. *Annu. Rev. Immunol.* **35**, 85–
594 118.

595 **Asha, H., de Ruiter, N., Wang, M. and Hariharan, I.** (1999). The Rap1 GTPase functions as a
596 regulator of morphogenesis invivo. *The EMBO Journal* **18**, 605–615.

597 **Bach, E. A., Ekas, L. A., Ayala-Camargo, A., Flaherty, M. S., Lee, H., Perrimon, N. and Baeg, G.-**
598 **H.** (2007). GFP reporters detect the activation of the Drosophila JAK/STAT pathway in
599 vivo. *Gene Expression Patterns* **7**, 323–331.

600 **Bai, J. and Montell, D.** (2002). Eyes Absent, a key repressor of polar cell fate during *Drosophila*
601 oogenesis. *Development* **129**, 5377–5388.

602 **Balaji, R., Weichselberger, V. and Classen, A.-K.** (2019). Response of epithelial cell and tissue
603 shape to external forces *in vivo*. *Development* dev.171256.

604 **Baum, J. S., Arama, E., Steller, H. and McCall, K.** (2007). The Drosophila caspases Strica and
605 Dronc function redundantly in programmed cell death during oogenesis. *Cell Death*
606 *Differ* **14**, 1508–1517.

607 **Beccari, S., Teixeira, L. and Rørth, P.** (2002). The JAK/STAT pathway is required for border cell
608 migration during Drosophila oogenesis. *Mechanisms of Development* **111**, 115–123.

609 **Besse, F. and Pret, A.-M.** (2003). Apoptosis-mediated cell death within the ovarian polar cell
610 lineage of *Drosophila melanogaster*. *Development* **130**, 1017–1027.

611 **Blanpain, C. and Fuchs, E.** (2009). Epidermal homeostasis: a balancing act of stem cells in the
612 skin. *Nat Rev Mol Cell Biol* **10**, 207–217.

613 **Boettner, B. and Van Aelst, L.** (2007). The Rap GTPase Activator *Drosophila* PDZ-GEF Regulates
614 Cell Shape in Epithelial Migration and Morphogenesis. *Mol Cell Biol* **27**, 7966–7980.

615 **Boettner, B., Harjes, P., Ishimaru, S., Heke, M., Fan, H. Q., Qin, Y., Van Aelst, L. and Gaul, U.**
616 (2003). The AF-6 Homolog Canoe Acts as a Rap1 Effector During Dorsal Closure of the
617 Drosophila Embryo. *Genetics* **165**, 159–169.

618 **Bonello, T. T., Perez-Vale, K. Z., Sumigray, K. D. and Peifer, M.** (2018). Rap1 acts via multiple
619 mechanisms to position Canoe/Afadin and adherens junctions and mediate apical-basal
620 polarity establishment. *Development* dev.157941.

621 **Borensztejn, A., Boissoneau, E., Fernandez, G., Agnès, F. and Pret, A.-M.** (2013). JAK/STAT
622 autocontrol of ligand-producing cell number through apoptosis. *Development* **140**, 195–
623 204.

624 **Borensztejn, A., Mascaro, A. and Wharton, K. A.** (2018). JAK/STAT signaling prevents excessive
625 apoptosis to ensure maintenance of the interfollicular stalk critical for Drosophila
626 oogenesis. *Developmental Biology* **438**, 1–9.

627 **Bröer, S.** (2008). Amino Acid Transport Across Mammalian Intestinal and Renal Epithelia.
628 *Physiological Reviews* **88**, 249–286.

629 **Cai, D., Dai, W., Prasad, M., Luo, J., Gov, N. S. and Montell, D. J.** (2016). Modeling and analysis
630 of collective cell migration in an in vivo three-dimensional environment. *Proc Natl Acad*
631 *Sci U S A* **113**, E2134-2141.

632 **Choi, W., Harris, N. J., Sumigray, K. D. and Peifer, M.** (2013). Rap1 and Canoe/afadin are
633 essential for establishment of apical–basal polarity in the *Drosophila* embryo. *MBoC* **24**,
634 945–963.

635 **Clem, R. J., Fechheimer, M. and Miller, L. K.** (1991). Prevention of Apoptosis by a Baculovirus
636 Gene During Infection of Insect Cells. *Science* **254**, 1388–1390.

637 **Crest, J., Diz-Muñoz, A., Chen, D.-Y., Fletcher, D. A. and Bilder, D.** (2017). Organ sculpting by
638 patterned extracellular matrix stiffness. *eLife* **6**, e24958.

639 **Duhart, J. C., Parsons, T. T. and Raftery, L. A.** (2017). The repertoire of epithelial
640 morphogenesis on display: Progressive elaboration of Drosophila egg structure.
641 *Mechanisms of Development* **148**, 18–39.

642 **Duszyc, K., Gomez, G. A., Schroder, K., Sweet, M. J. and Yap, A. S.** (2017). In life there is death:
643 How epithelial tissue barriers are preserved despite the challenge of apoptosis. *Tissue*
644 *Barriers* **5**, e1345353.

645 **Gloerich, M. and Bos, J. L.** (2011). Regulating Rap small G-proteins in time and space. *Trends in*
646 *Cell Biology* **21**, 615–623.

647 **Guillot, C. and Lecuit, T.** (2013). Mechanics of Epithelial Tissue Homeostasis and
648 Morphogenesis. *Science* **340**, 1185–1189.

649 **Haigo, S. L. and Bilder, D.** (2011). Global Tissue Revolutions in a Morphogenetic Movement
650 Controlling Elongation. *Science* **331**, 1071–1074.

651 **Haigo, S. L., Hildebrand, J. D., Harland, R. M. and Wallingford, J. B.** (2003). Shroom Induces
652 Apical Constriction and Is Required for Hingepoint Formation during Neural Tube
653 Closure. *Current Biology* **13**, 2125–2137.

654 **Harris, T. J. C. and Tepass, U.** (2010). Adherens junctions: from molecules to morphogenesis.
655 *Nat Rev Mol Cell Biol* **11**, 502–514.

656 **Hay, B. A., Wolff, T. and Rubin, G. M.** (1994). Expression of baculovirus P35 prevents cell death
657 in Drosophila. *Development* **120**, 2121–2129.

658 **Hay, B. A., Wassarman, D. A. and Rubin, G. M.** (1995). Drosophila homologs of baculovirus
659 inhibitor of apoptosis proteins function to block cell death. *Cell* **83**, 1253–1262.

660 **Irvine, K. D. and Wieschaus, E.** (1994). Cell intercalation during Drosophila germband extension
661 and its regulation by pair-rule segmentation genes. *Development* **120**, 827–841.

662 **Keller, R. E.** (1981). An experimental analysis of the role of bottle cells and the deep marginal
663 zone in gastrulation ofXenopus laevis. *J. Exp. Zool.* **216**, 81–101.

664 **Khammari, A., Agnès, F., Gandille, P. and Pret, A.-M.** (2011). Physiological apoptosis of polar
665 cells during Drosophila oogenesis is mediated by Hid-dependent regulation of Diap1.
666 *Cell Death Differ* **18**, 793–805.

667 **Kim, Y. S., Fan, R., Lith, S. C., Dicke, A.-K., Drexler, H. C. A., Kremer, L., Kuempel-Rink, N.,**
668 **Hekking, L., Stehling, M. and Bedzhov, I.** (2022). Rap1 controls epiblast morphogenesis
669 in sync with the pluripotency states transition. *Developmental Cell* **57**, 1937-1956.e8.

670 **Knox, A. L. and Brown, N. H.** (2002). Rap1 GTPase Regulation of Adherens Junction Positioning
671 and Cell Adhesion. *Science* **295**, 1285–1288.

672 **Lebo, D. P. V. and McCall, K.** (2021). Murder on the Ovarian Express: A Tale of Non-
673 Autonomous Cell Death in the Drosophila Ovary. *Cells* **10**, 1454.

674 **Li, M., Sun, S., Priest, J., Bi, X. and Fan, Y.** (2019). Characterization of TNF-induced cell death in
675 Drosophila reveals caspase- and JNK-dependent necrosis and its role in tumor
676 suppression. *Cell Death Dis* **10**, 613.

677 **Loyer, N., Kolotuev, I., Pinot, M. and Le Borgne, R.** (2015). *Drosophila* E-cadherin is required for
678 the maintenance of ring canals anchoring to mechanically withstand tissue growth. *Proc.*
679 *Natl. Acad. Sci. U.S.A.* **112**, 12717–12722.

680 **Martin, A. C. and Goldstein, B.** (2014). Apical constriction: themes and variations on a cellular
681 mechanism driving morphogenesis. *Development* **141**, 1987–1998.

682 **Martin, A. C., Kaschube, M. and Wieschaus, E. F.** (2009). Pulsed contractions of an actin–
683 myosin network drive apical constriction. *Nature* **457**, 495–499.

684 **Munjal, A. and Lecuit, T.** (2014). Actomyosin networks and tissue morphogenesis. *Development*
685 **141**, 1789–1793.

686 **Niewiadomska, P., Godt, D. and Tepass, U.** (1999). DE-Cadherin Is Required for Intercellular
687 Motility during Drosophila Oogenesis. *Journal of Cell Biology* **144**, 533–547.

688 **Osswald, M., Barros-Carvalho, A., Carmo, A. M., Loyer, N., Gracio, P. C., Sunkel, C. E., Homem,**
689 **C. C. F., Januschke, J. and Morais-de-Sá, E.** (2022). aPKC regulates apical constriction to
690 prevent tissue rupture in the Drosophila follicular epithelium. *Current Biology*
691 S0960982222013859.

692 **Peifer, M., Orsulic, S., Sweeton, D. and Wieschaus, E.** (1993). A role for the Drosophila segment
693 polarity gene armadillo in cell adhesion and cytoskeletal integrity during oogenesis.
694 *Development* **118**, 1191–1207.

695 **Perez-Vale, K. Z., Yow, K. D., Johnson, R. I., Byrnes, A. E., Finegan, T. M., Slep, K. C. and Peifer,**
696 **M.** (2021). Multivalent interactions make adherens junction–cytoskeletal linkage robust
697 during morphogenesis. *Journal of Cell Biology* **220**, e202104087.

698 **Perez-Vale, K. Z., Yow, K. D., Gurley, N. J., Greene, M. and Peifer, M.** (2022). Rap1 regulates
699 apical contractility to allow embryonic morphogenesis without tissue disruption and
700 acts in part via Canoe-independent mechanisms. *MBoC* mbc.E22-05-0176.

701 **Potla, U., Ni, J., Vadaparampil, J., Yang, G., Leventhal, J. S., Campbell, K. N., Chuang, P. Y.,**
702 **Morozov, A., He, J. C., D'Agati, V. D., et al.** (2014). Podocyte-specific RAP1GAP
703 expression contributes to focal segmental glomerulosclerosis–associated glomerular
704 injury. *J. Clin. Invest.* **124**, 1757–1769.

705 **Royou, A., Field, C., Sisson, J. C., Sullivan, W. and Karess, R.** (2004). Reassessing the Role and
706 Dynamics of Nonmuscle Myosin II during Furrow Formation in Early *Drosophila* Embryos.
707 *MBoC* **15**, 838–850.

708 **Ruohola, H., Bremer, K. A., Baker, D., Swedlow, J. R., Jan, L. Y. and Jan, Y. N.** (1991). Role of
709 neurogenic genes in establishment of follicle cell fate and oocyte polarity during
710 oogenesis in Drosophila. *Cell* **66**, 433–449.

711 **Sarpal, R., Pellikka, M., Patel, R. R., Hui, F. Y. W., Godt, D. and Tepass, U.** (2012). Mutational
712 analysis supports a core role for *Drosophila* α-Catenin in adherens junction function.
713 *Journal of Cell Science* **125**, 233–245.

714 **Sasaki, K., Kojitani, N., Hirose, H., Yoshihama, Y., Suzuki, H., Shimada, M., Takayanagi, A.,**
715 **Yamashita, A., Nakaya, M., Hirano, H., et al.** (2020). Shank2 Binds to aPKC and Controls
716 Tight Junction Formation with Rap1 Signaling during Establishment of Epithelial Cell
717 Polarity. *Cell Reports* **31**, 107407.

718 **Sawant, K., Chen, Y., Kotian, N., Preuss, K. M. and McDonald, J. A.** (2018). Rap1 GTPase
719 promotes coordinated collective cell migration in vivo. *MBoC* **29**, 2656–2673.

720 **Sawyer, J. K., Harris, N. J., Slep, K. C., Gaul, U. and Peifer, M.** (2009). The Drosophila afadin
721 homologue Canoe regulates linkage of the actin cytoskeleton to adherens junctions
722 during apical constriction. *Journal of Cell Biology* **186**, 57–73.

723 **Silver, D. L. and Montell, D. J.** (2001). Paracrine Signaling through the JAK/STAT Pathway
724 Activates Invasive Behavior of Ovarian Epithelial Cells in Drosophila. *Cell* **107**, 831–841.

725 **Spahn, P., Ott, A. and Reuter, R.** (2012). The PDZ-GEF Dizzy regulates the establishment of
726 adherens junctions required for ventral furrow formation in *Drosophila*. *Journal of Cell*
727 *Science* jcs.101196.

728 **Spradling A. C.** (1993). Developmental genetics of oogenesis. In *The Development of*
729 *Drosophila Melanogaster*, pp. 1-70. CSHL Press.
730
731 **Starz-Gaiano, M., Melani, M., Wang, X., Meinhardt, H. and Montell, D. J.** (2008). Feedback
732 Inhibition of JAK/STAT Signaling by Apontic Is Required to Limit an Invasive Cell
733 Population. *Developmental Cell* **14**, 726–738.

734 **Stonko, D. P., Manning, L., Starz-Gaiano, M. and Peercy, B. E.** (2015). A mathematical model of
735 collective cell migration in a three-dimensional, heterogeneous environment. *PLoS One*
736 **10**, e0122799.

737 **Tai, K., Cockburn, K. and Greco, V.** (2019). Flexibility sustains epithelial tissue homeostasis.
738 *Current Opinion in Cell Biology* **60**, 84–91.

739 **Wang, Y.-C., Khan, Z. and Wieschaus, E. F.** (2013). Distinct Rap1 Activity States Control the
740 Extent of Epithelial Invagination via α-Catenin. *Developmental Cell* **25**, 299–309.

741 **Wang, A., Dunn, A. R. and Weis, W. I.** (2022). Mechanism of the cadherin–catenin F-actin catch
742 bond interaction. *eLife* **11**, e80130.

743 **Williams-Masson, E. M., Malik, A. N. and Hardin, J.** (1997). An actin-mediated two-step
744 mechanism is required for ventral enclosure of the C. elegans hypodermis. *Development*
745 **124**, 2889–2901.

746 **Yan, N., Wu, J.-W., Chai, J., Li, W. and Shi, Y.** (2004). Molecular mechanisms of DrICE inhibition
747 by DIAP1 and removal of inhibition by Reaper, Hid and Grim. *Nat Struct Mol Biol* **11**,
748 420–428.

749 **Yonemura, S., Wada, Y., Watanabe, T., Nagafuchi, A. and Shibata, M.** (2010). α-Catenin as a
750 tension transducer that induces adherens junction development. *Nat Cell Biol* **12**, 533–
751 542.

752

753

754

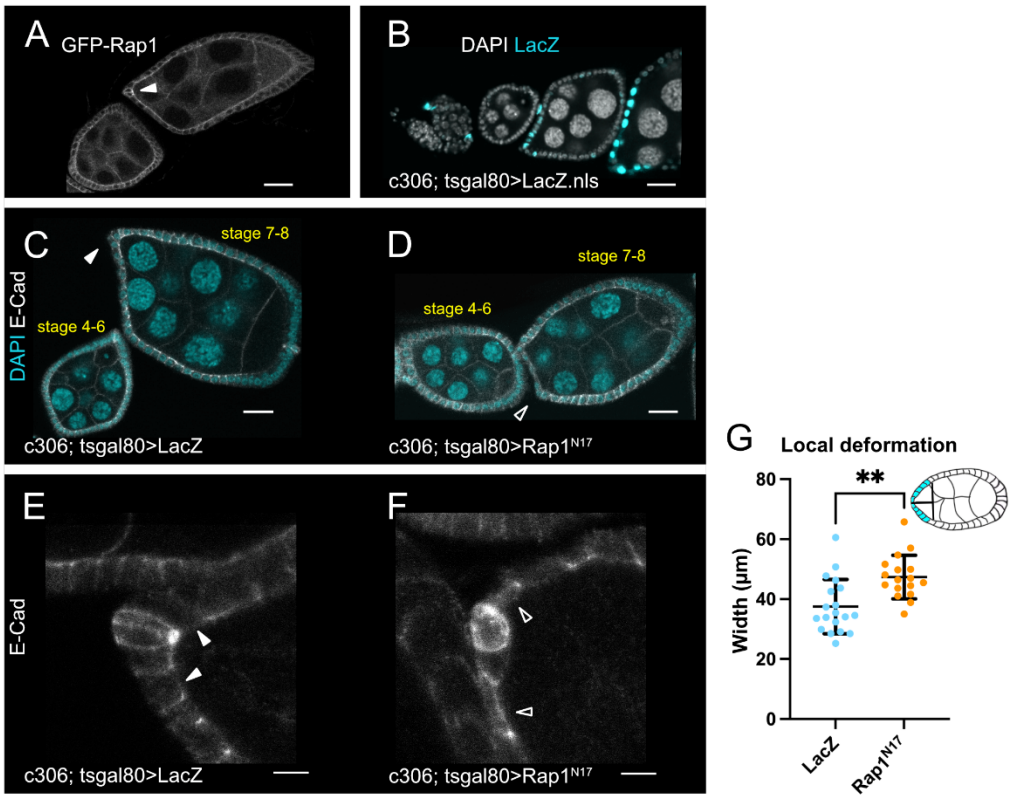

Figure 1. Rap1 is required in the anterior epithelium to maintain follicle cell and egg chamber shapes

(A) Ovariole with GFP tagged Rap1 illustrates Rap1 enrichment in follicle cells. Arrowhead indicates apical Rap1 accumulation in anterior epithelium. (B) Ovariole expressing UAS-LacZ driven by *c306*-GAL4 to demonstrate the *c306*-GAL4 expression pattern. (C-D) LacZ control (C) or DN-Rap1^{N17} (D) egg chambers. Anterior epithelia are distorted at stages 7-8 in DN-Rap1^{N17}. Arrowheads indicate anterior region of stage 7-8 egg chambers. Solid arrowhead points to normal anterior epithelium of control (C), while open arrowhead indicates distorted anterior region for DN-Rap1^{N17} (D). (E-F) Anterior regions of stage 7-8 egg chambers showing normal cuboidal epithelium in control (E) or stretched cell shapes in DN-Rap1^{N17} (F). Solid arrowheads indicate cuboidal shaped cells in E. Open arrowheads indicate stretched cells in F. (G) Quantification of local deformation measures taken at 20% of egg chamber length (illustrated by egg chamber schematic in G). ** $p \leq 0.01$ two-tailed unpaired t-test. $N \geq 17$ egg chambers measured per genotype. (A-D) Scale bars 20µm. (E-F) Scale bars 5µm. Anterior is to the left in this and the following figures.

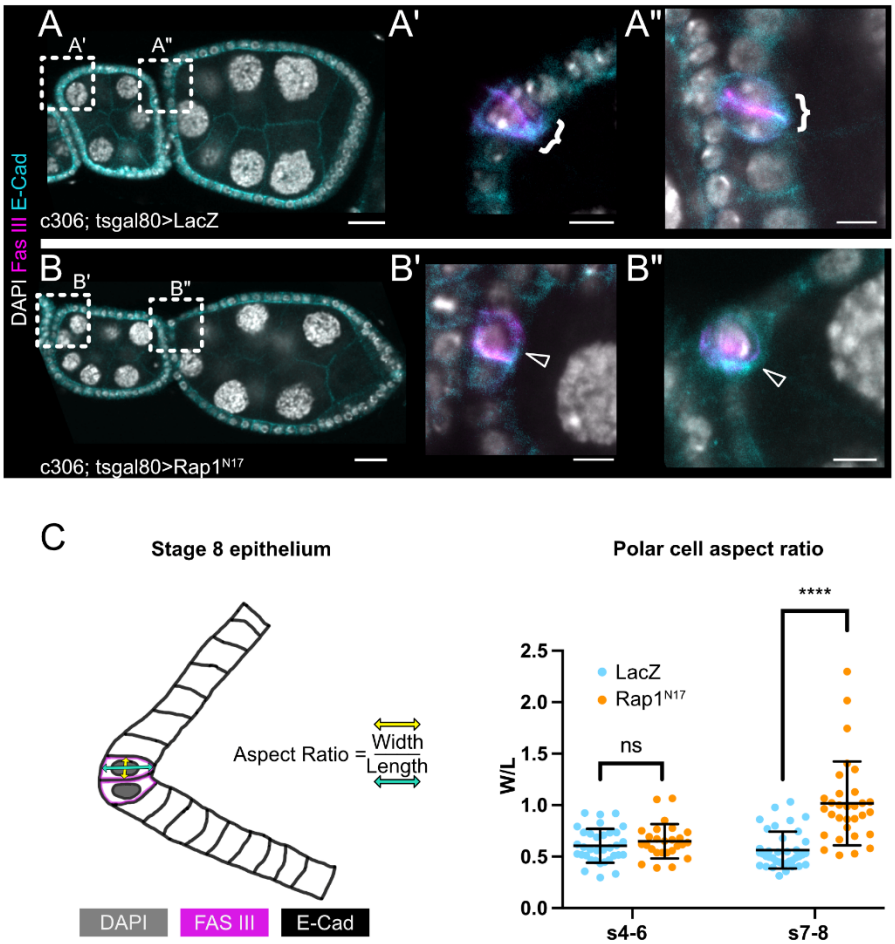

Figure 2. Rap1 is required for proper polar cell shape

(A-B) LacZ (A) and DN-Rap1^{N17} (B) ovarioles imaged for polar cell shape. Dashed boxes indicate the regions expanded in A', A", B', and B". (A'-A", B'-B") Close-up views of anterior egg chamber regions. Control stage 4-6 (A') and stage 7-8 (A") egg chamber polar cells. Brackets indicate intact polar cell pairs. (B'-B") DN-Rap1^{N17} stage 4-6 (B') and stage 7-8 (B") egg chamber polar cells. (B') Only one polar cell is present at stage 4-6. (B") One spherical polar cell is present at stage 7-8. Open arrowheads indicate only one polar cell is present. (C) Aspect ratio schematic and quantification. Aspect ratio (AR) was defined as the dorsoventral (DV, yellow arrow) width divided by the anterior-posterior (AP, cyan arrow) length. AR measurements plotted for stage 4-6 and stage 7-8 egg chamber polar cells. DN-Rap1^{N17} polar cells are more spherical at stage 7-8 indicated by average AR=1.02 vs average AR=0.56 for control. **** $p \leq 0.0001$ two-tailed unpaired t test. N≥26 polar cells measured per genotype per egg chamber stage. (A-B) Scale bars 20μm. (A'-B") Scale bars 5μm.

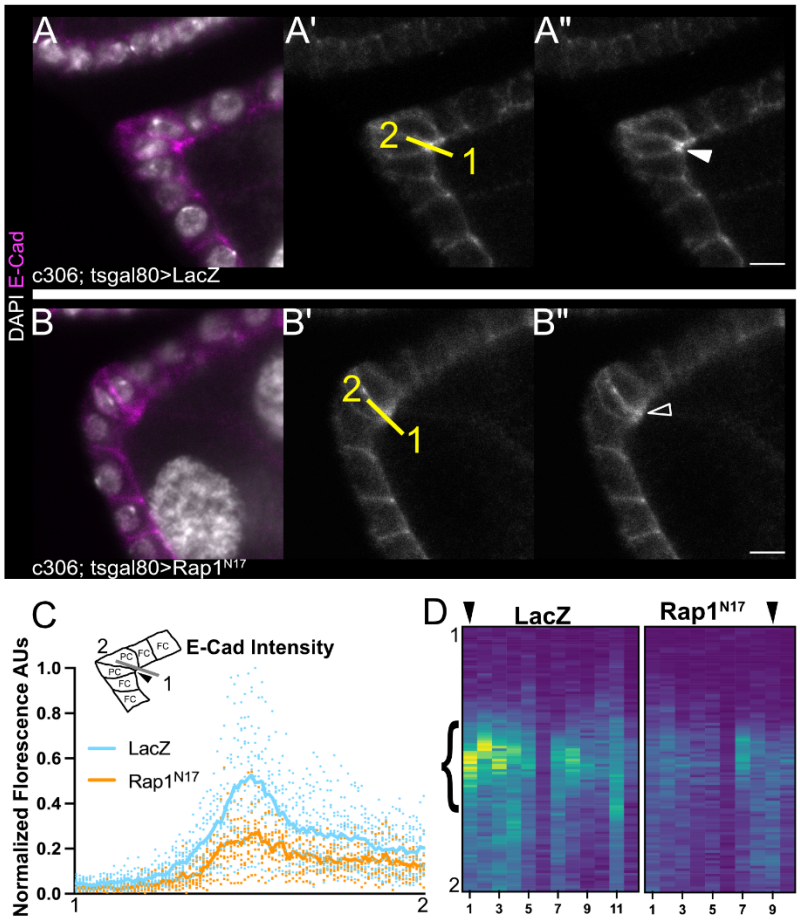

Figure 3. Rap1 is required for apical E-Cadherin enrichment in polar cells

(A-B) Anterior regions of stage 7-8 egg chambers for LacZ control (A) and DN-Rap1^{N17} egg chambers (B). (A'-B") Single channel panels of A and B showing E-Cadherin (gray) enrichment. (A', B') Yellow line indicates region of measurement beginning over nurse cells (1) and ending along lateral polar cell-polar cell interface (2). Solid arrowhead indicates apical accumulation of E-Cadherin. Open arrowhead indicates reduced E-Cadherin enrichment. (A", B") Same as A' and B' without line overlays for clarity. Image brightness adjusted for presentation purposes. (C) Measurement schematic and quantification of fluorescence intensities measured along lines drawn as in A' and B' and normalized to highest signal. Lines represent mean intensity. (D) Heat map representation of C. Bracket indicates area of heat map corresponding to apical enrichment of E-Cadherin in polar cells. Arrowheads at the top of heat map indicate the lanes corresponding to A" and B". Scale bars 5μm.

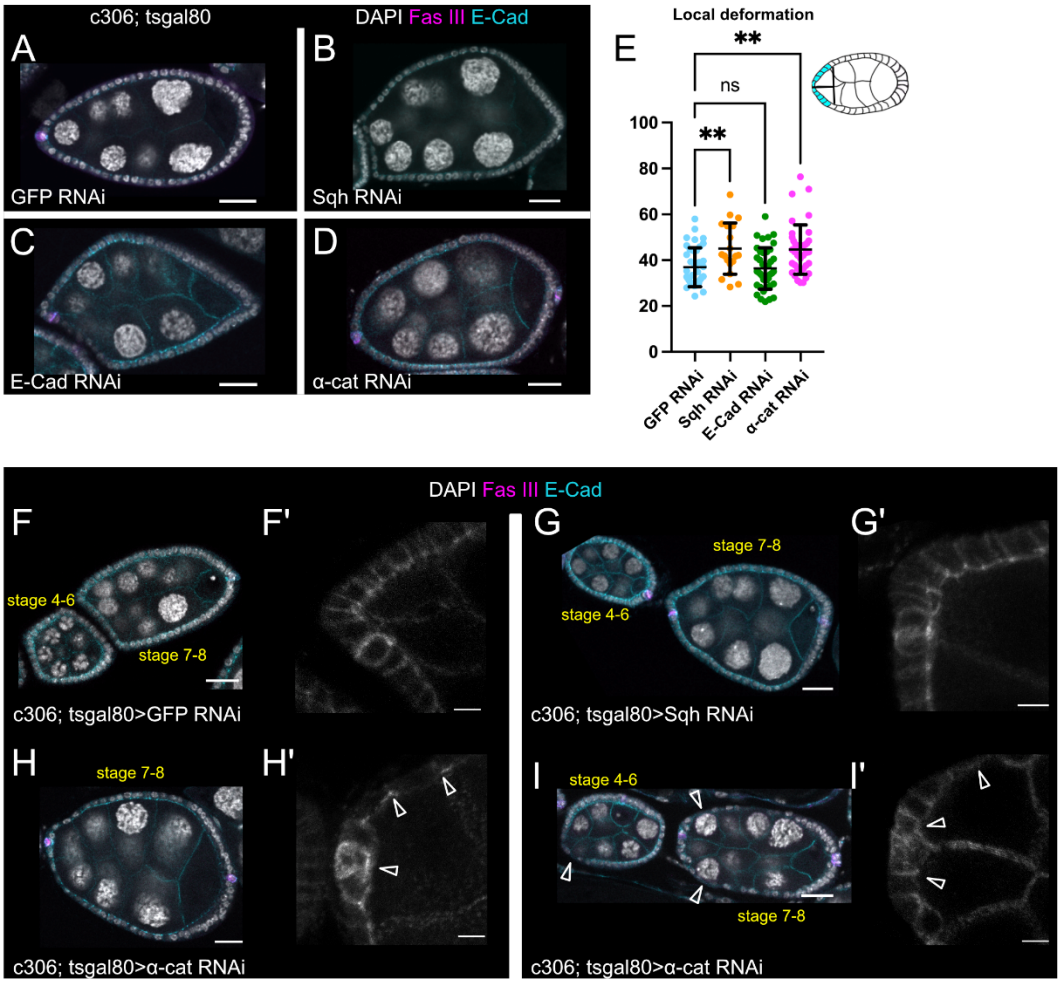

Figure 4. Sqh and α-Catenin maintain local tissue shape and α-Catenin is required for epithelial integrity

(A-D) Stage 7-8 GFP RNAi (A), Sqh RNAi, (B) E-Cadherin RNAi (C), and α-cat RNAi (D) egg chambers imaged for egg chamber shape. (E) Schematic and quantification of local deformation measurement. ** $p \leq 0.01$ One-way ANOVA followed by Dunnett's multiple comparisons test. $N \geq 19$ egg chambers per genotype. (F-I) GFP RNAi (F), Sqh RNAi (G), and α-cat RNAi (H-I) ovarioles imaged to show egg chamber shape and anterior epithelium. (F'-I') Maximum intensity projections of anterior regions of stage 7-8 egg chambers pictured in the main panels. Open arrowheads in H', I, and I' indicate "stretched" or clustered cells observed in α-cat RNAi egg chambers. (A-D, F-I) Scale bars 20μm. (F'-I') Scale bars 5μm.

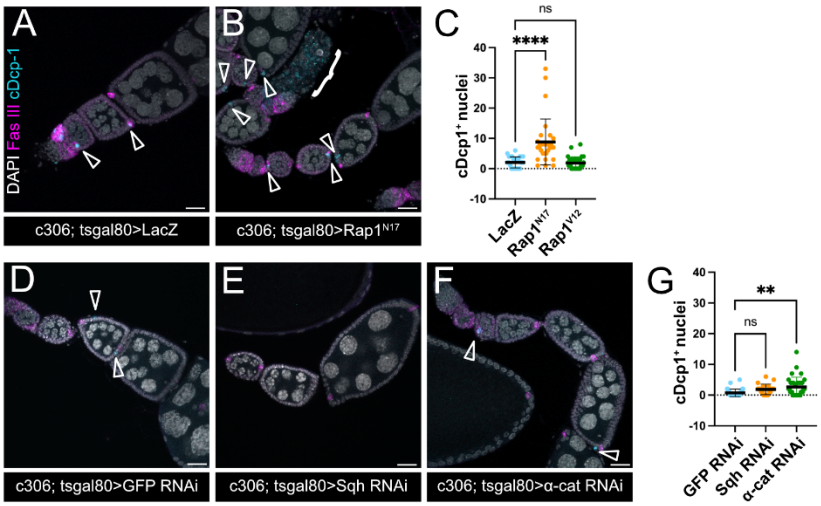

Figure 5. Rap1 and α-Catenin are required for cell viability during oogenesis

(A-B) Maximum intensity projections of ovarioles showing caspase positive nuclei for LacZ (A) and DN-Rap1^{N17} (B). Open arrowheads in A and B indicate cDcp1 positive nuclei and the bracket in B indicates a degenerating egg chamber. (C) Quantification of cDcp1 positive nuclei per ovariole (egg chamber stages 2-8 only). DN-Rap1^{N17} ovarioles have greater number of cDcp1 positive nuclei. **** $p \leq 0.0001$ One-way ANOVA followed by Dunnett's multiple comparisons test. N≥29 ovarioles per genotype. (D-F) Maximum intensity projections of ovarioles for GFP RNAi (D), Sqh RNAi (E), and α-cat RNAi (F). Open arrowheads indicate cDcp1 positive nuclei. (G) Quantification of cDcp1 positive nuclei. ** $p \leq 0.01$ One-way ANOVA followed by Dunnett's multiple comparisons test. N≥20 ovarioles per genotype. Scale bars 20μm.

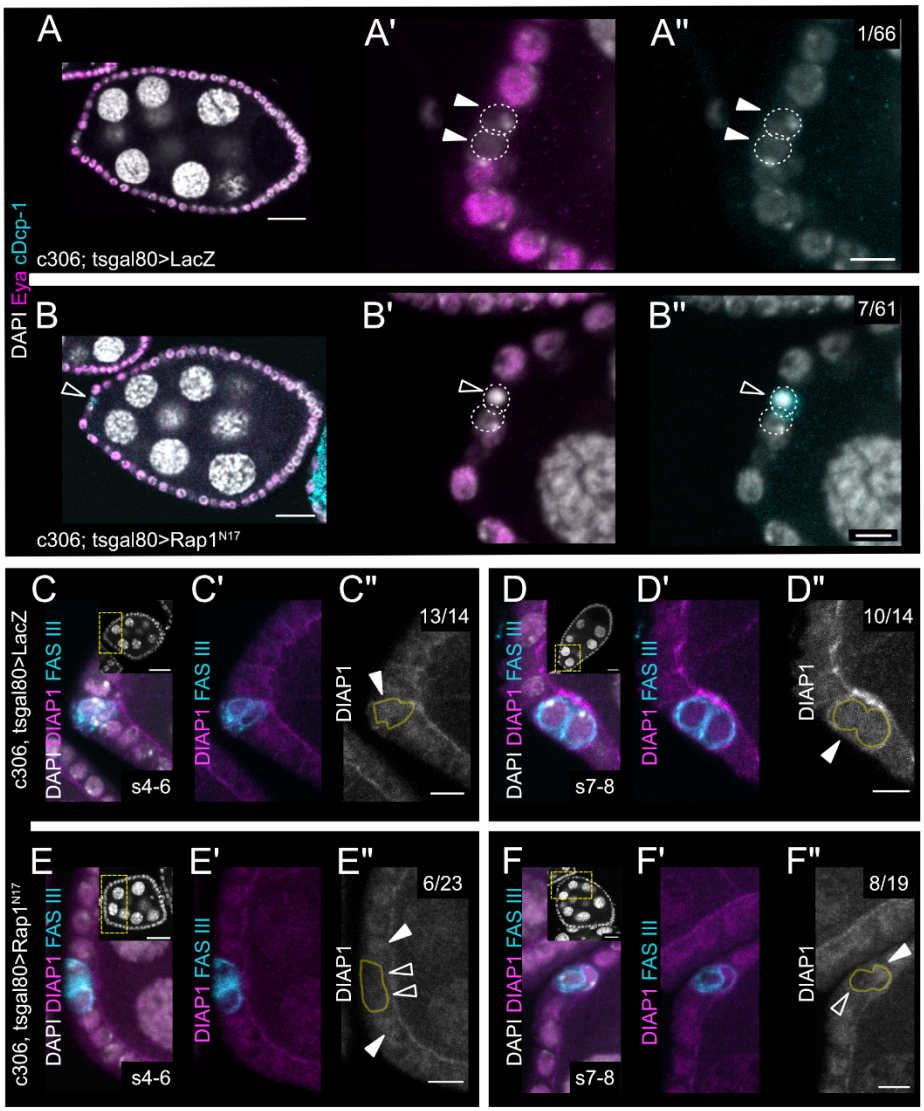

Figure 6. Rap1 is required for polar cell viability and proper DIAP1 accumulation

(A-B) Stage 7-8 LacZ (A) and DN-Rap1^{N17} (B) egg chambers scored for cDcp1 positive polar cells . (A', B') Close-up views of anterior regions of the egg chambers depicted in A and B, showing only DAPI and Eya staining. (A", B") Same images as A' and B' showing only DAPI and cDcp1. Filled arrowheads in A' and A" indicate viable mature polar cells. Open arrowheads in B' and B" indicate a cDcp1 positive dying polar cell. Numbers in A" and B" indicate number of observations of cDcp1 positive polar cells per stage 7-8 egg chambers scored. (C-C", E-E") Stage 4-6 LacZ (C-C") and DN-Rap1^{N17} (E-E") egg chambers. (C', E') Same images as C and E showing only DIAP1 and FasIII. (C", E") DIAP1 only. (D-D", F-F") Stage 7-8 LacZ (D-D") and DN-Rap1^{N17} (F-F") egg chambers. (C-F) Insets show DAPI-stained whole egg chambers corresponding to zoomed regions with yellow boxes outlining the approximate region depicted in main panels. (C"-F") Polar cells are outlined in yellow. Solid arrowheads indicate normal DIAP1

841 accumulation. Open arrowheads indicate reduced DIAP1. The number of egg chambers with
842 normal DIAP1 accumulation out of total egg chambers scored is reported in the upper right of
843 C”, D”, E”, and F”. (A-F) Scale bars 20μm. (C”-F”) Scale bars 5μm.
844

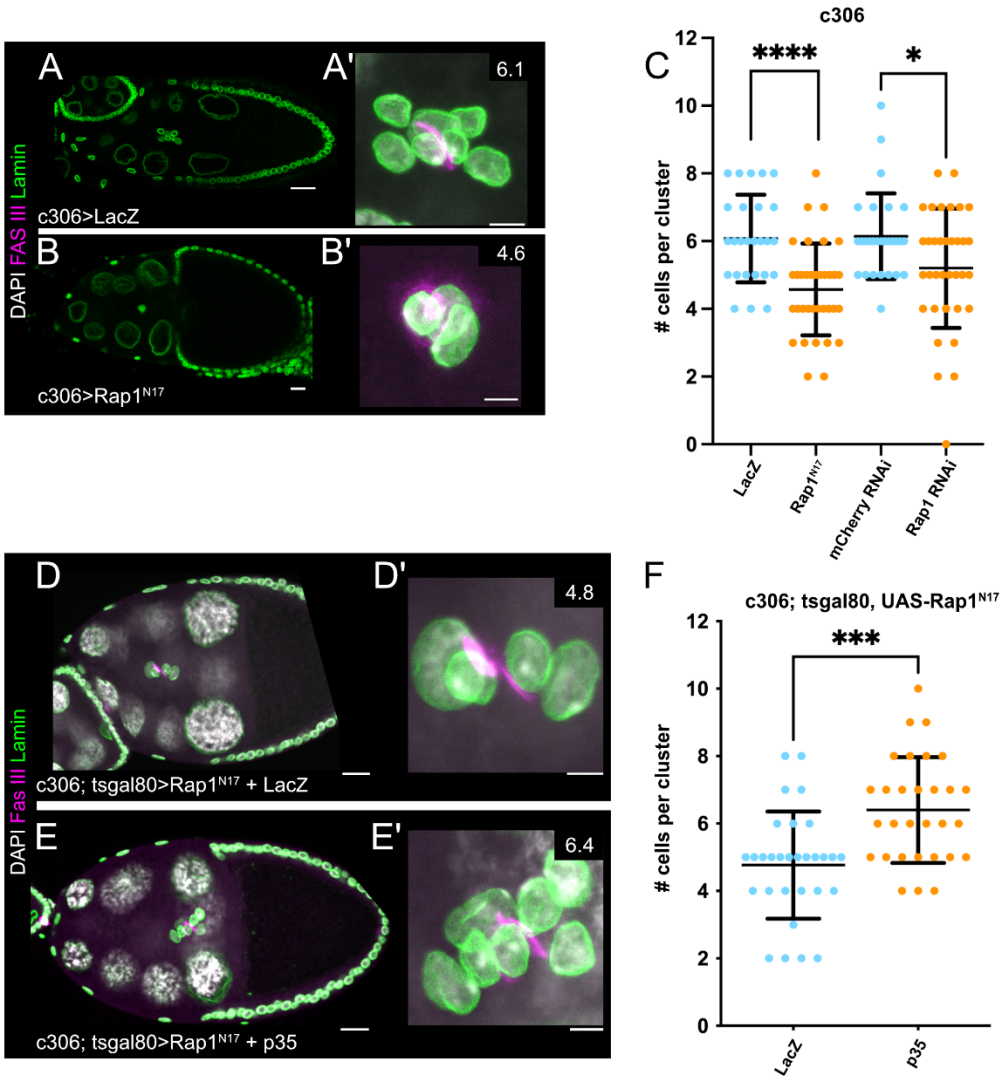

Figure 7. Rap1 dependent cell viability is required for proper border cell cluster assembly (A-B) Stage 9-10 egg chambers for LacZ (A) and DN-Rap1^{N17} (B). (A'-B') Maximum intensity projections of border cell clusters from egg chambers pictured in A and B. Numbers at top right are average number of cells observed for each genotype. (C) Quantification of cell number per cluster for each genotype. * $p \leq 0.05$ ****$p \leq 0.0001$ two-tailed unpaired t test. N≥26 border cell clusters per genotype. (D-E) Stage 9-10 egg chambers for DN-Rap1^{N17} + LacZ expression control (D) or DN-Rap1^{N17} + p35 (E). (D'- E') Maximum intensity projections of border cell clusters from egg chambers pictured in D and E. Numbers at top right are average number of cells observed for each genotype. (F) Quantification of cell number per cluster for each genotype. *** $p \leq 0.001$ two-tailed unpaired t test. N=30 border cell clusters per genotype. (A-B, D-E) Scale bars 20μm. (A'-B', D'-E') Scale bars 5μm.

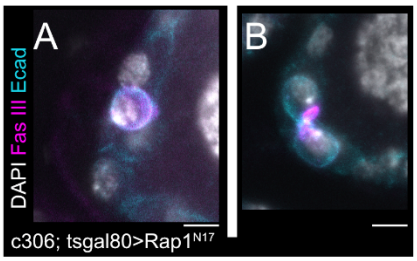

858

859 **Figure S1. Rap1 inhibition causes polar cell loss and distorted polar cell shapes**

860 (A-B) Anterior regions of two different DN-Rap1^{N17} stage 7-8 egg chambers. (A) Only one

861 mature polar cell is present. (B) A pair of polar cells stretched along the dorsoventral axis. Scale

862 bars 5μm.

863

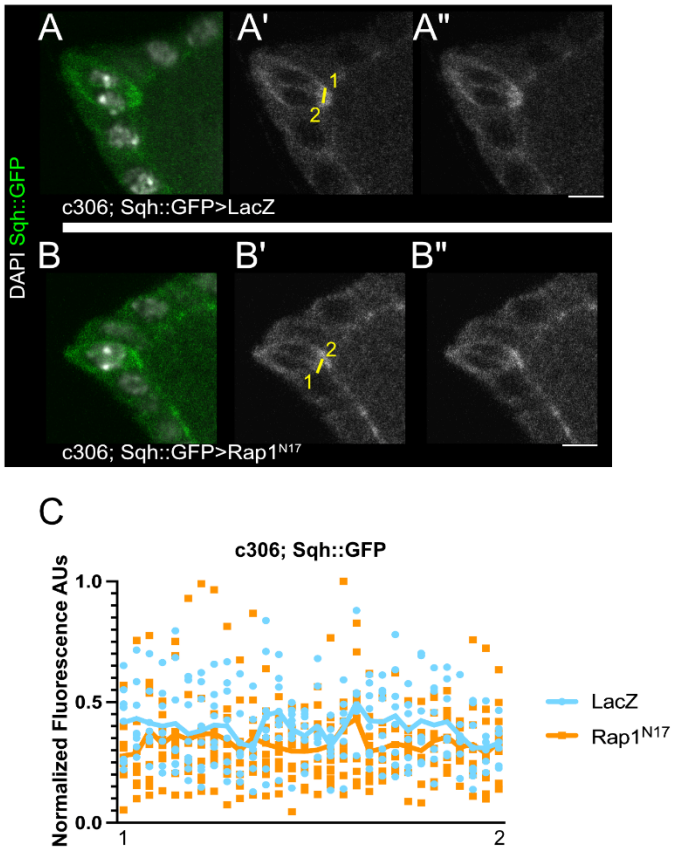

Figure S2. Rap1 is dispensable for Sqh apical localization in polar cells

(A-B) Anterior regions of stage 7-8 egg chambers for LacZ (A) or DN-Rap1^{N17} (B). (A'-B') Single channel images of A and B showing GFP (gray) with yellow lines indicating region of measurement for Sqh::GFP intensity. The numbers correspond to the plot intensity profiles in C. (A"-B") Single channel images as in A' and B' with line removed for clarity. The image brightness was adjusted for presentation purposes but not used for quantification. (C) Profile of the intensity values along the measurement lines, plotted and normalized to highest signal. The numbers on the x-axis correspond to the lines drawn on A' and B'. Solid plot lines represent the mean intensity. N ≥ 8 egg chambers per genotype. Scale bars 5μm.

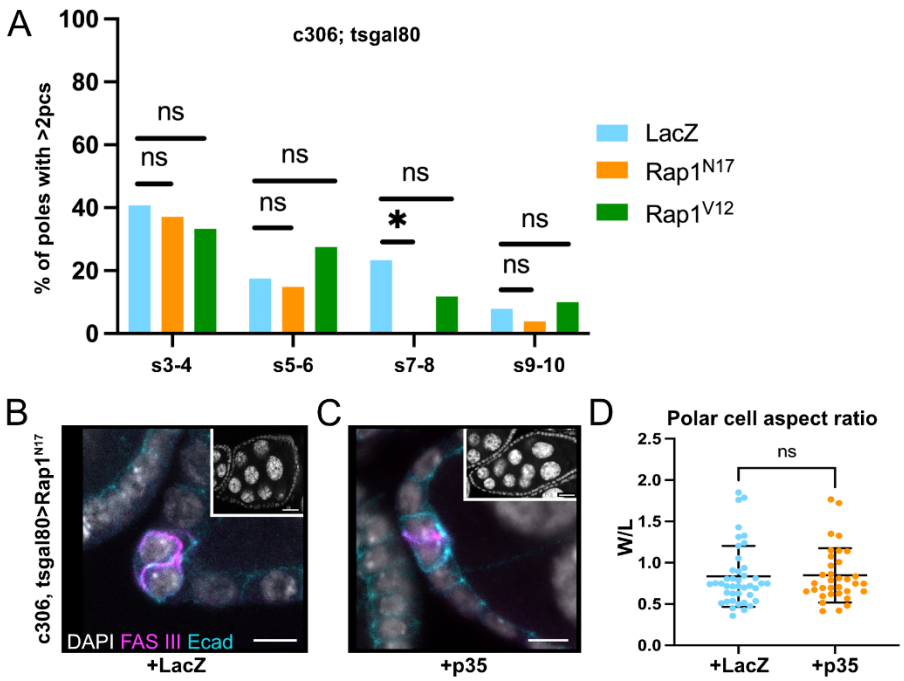

Figure S3. Rap1 does not regulate early elimination of supernumerary polar cells and maintains mature polar cell shape independent of apoptosis

(A) Quantification showing frequency of egg chamber poles with supernumerary polar cells during specific stages of oogenesis. * $p \leq 0.05$ two-sided Fisher's exact test. N≥30 egg chamber poles per stage per genotype. Supernumerary polar cells are present early for all genotypes. (B-C) Anterior region of stage 7-8 egg chambers, DN-Rap1^{N17} with LacZ expression (A) or DN-Rap1^{N17} with apoptosis inhibitor p35 (B). Whole egg chambers stained for DAPI are shown in the insets. (D) Polar cell aspect ratio quantification. Mean AR of DN-Rap1^{N17} + LacZ control = 0.84. Mean AR of DN-Rap1^{N17} + p35 = 0.85. NS two-tailed unpaired t test. N≥34 polar cells per genotype. Main panel scale bars 5μm. Inset scale bars 20μm.

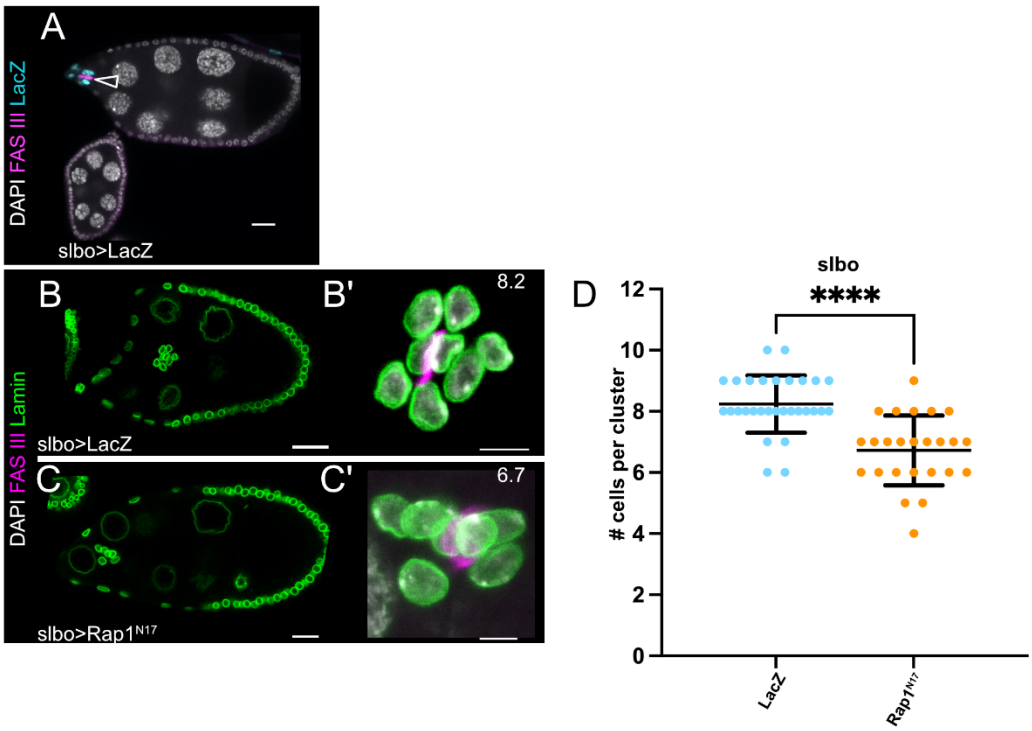

887

888 **Figure S4. Effects of late Rap1 inhibition on border cell numbers**

889 (A) Ovariole region expressing UAS-LacZ indicates the expression pattern of *slbo*-GAL4. (B-C)
890 Stage 9-10 LacZ (B) and DN-Rap1^{N17} (C) egg chambers showing mid-migration border cells.
891 (B'-C') Maximum intensity projections of border cell clusters from B and C. Numbers in the
892 upper right indicate the average number of cells per cluster. (D) Quantification of cell number
893 per cluster for Rap1 inhibition using *slbo*-GAL4. **** $p \leq 0.0001$ two-tailed unpaired t test. $N \geq 25$
894 border cell clusters per genotype. (A-C) Scale bars 20μm. (B'-C') Scale bars 5μm.

895

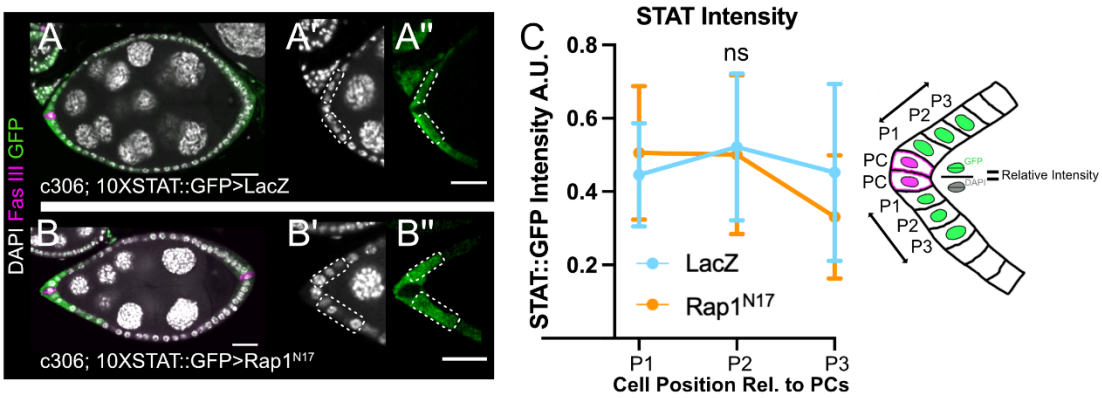

Figure S5. Rap1 is dispensable for STAT levels in follicle cells fated to become border cells

(A, B) Stage 8 LacZ (A) and DN-Rap1^{N17} (B) egg chambers with 10XSTAT::GFP reporter expression enriched adjacent to anterior polar cells. (A'-A", B'-B") Insets of the anterior end of the egg chambers in A and B, which was used to measure the intensity of nuclear 10XSTAT::GFP. (A'-B') DAPI. (A"-B") 10XSTAT::GFP. Dashed rectangles indicate the cell positions next to polar cells used for analyzing STAT levels. (C) Schematic and plot of STAT intensity values relative to the DAPI signal and normalized to the highest intensity STAT measurement. NS, unpaired two-tailed t-test. N≥12 follicle cells at each position pooled from N≥6 stage 8 egg chambers for each genotype. (A-B) Scale bars 20μm. (A"-B") Scale bars 5μm.

908 **Table 1. Fly strains used in this study.**

Fly Stock	Source	Appears in Figures
c306-GAL4		7
c306-GAL4; 10XSTAT92E-GFP	M. Starz-Gaiano	S5
c306-GAL4; UAS-Rap1N17, tsgal80	This study	7, S3
c306-GAL4; Sqh::GFP	P. Majumder	S2
c306-GAL4; tsgal80	P. Majumder	1, 2, 3, 4, 5, 6, S1, S3
c306-GAL4, tsgal80; PT Fas III (GFP)	This study	6
slbo-GAL4	BDSC 58435	S4
GFP-Rap1	N. Brown	1
UAS-α-Catenin RNAi	VDRC v107298	4, 5
UAS-E-Cadherin RNAi	VDRC v103962	4
UAS-GFP RNAi	VDRC v60102	4, 5
UAS-LacZ.nls	D. Montell	1, 2, 3, 5, 6, 7, S2, S3, S4, S5
UAS-mCherry RNAi	BDSC 35785	7
UAS-p35.H	BDSC 5072	7, S3
UAS-Rap1N17	B. Boettner	1, 2, 3, 5, 6, 7, S1, S2, S3, S4, S5
UAS-Rap1 RNAi	VDRC v33437	7
UAS-Rap1V12	B. Boettner	5, S3
UAS-Sqh RNAi	VDRC v7916	4, 5

909

910

911 **Table 2. Genotypes in this study.**

Figure	Genotypes
1A	w; P[w+ GFP-Rap1]
1B	c306-GAL4/w; tsgal80/+; UAS-LacZ.nls/+
1C	c306-GAL4/w; tsgal80/+; UAS-LacZ.nls/+
1D	c306-GAL4/w; tsgal80/UAS-Rap1N17; TM2/+
1E	c306-GAL4/w; tsgal80/+; UAS-LacZ.nls/+
1F	c306-GAL4/w; tsgal80/UAS-Rap1N17; TM2/+
1G	c306-GAL4/w; tsgal80/+; UAS-LacZ.nls/+ c306-GAL4/w; tsgal80/UAS-Rap1N17; TM2/+
2A-A"	c306-GAL4/w; tsgal80/+; UAS-LacZ.nls/+
2B-B"	c306-GAL4/w; tsgal80/UAS-Rap1N17; TM2/+
2C	c306-GAL4/w; tsgal80/+; UAS-LacZ.nls/+ c306-GAL4/w; tsgal80/UAS-Rap1N17; TM2/+
3A-A"	c306-GAL4/w; tsgal80/+; UAS-LacZ.nls/+
3B-B"	c306-GAL4/w; tsgal80/UAS-Rap1N17; TM2/+
3C-D	c306-GAL4/w; tsgal80/+; UAS-LacZ.nls/+ c306-GAL4/w; tsgal80/UAS-Rap1N17; TM2/+
4A	c306-GAL4/w; tsgal80/UAS-GFP-RNAi
4B	c306-GAL4/w; tsgal80/UAS-Sqh-RNAi
4C	c306-GAL4/w; tsgal80/UAS-E-Cadherin-RNAi
4D	c306-GAL4/w; tsgal80/UAS-α-Catenin-RNAi
4E	c306-GAL4/w; tsgal80/UAS-GFP-RNAi c306-GAL4/w; tsgal80/UAS-Sqh-RNAi c306-GAL4/w; tsgal80/UAS-E-Cadherin-RNAi c306-GAL4/w; tsgal80/UAS-α-Catenin-RNAi
4F-F'	c306-GAL4/w; tsgal80/UAS-GFP-RNAi
4G-G'	c306-GAL4/w; tsgal80/UAS-Sqh-RNAi
4H-H'	c306-GAL4/w; tsgal80/UAS-α-Catenin-RNAi
4I-I'	c306-GAL4/w; tsgal80/UAS-α-Catenin-RNAi
5A	c306-GAL4/w; tsgal80/+; UAS-LacZ.nls/+
5B	c306-GAL4/w; tsgal80/UAS-Rap1N17; TM2/+
5C	c306-GAL4/w; tsgal80/+; UAS-LacZ.nls/+ c306-GAL4/w; tsgal80/UAS-Rap1N17; TM2/+ c306-GAL4/w; tsgal80/BL; UAS-Rap1V12/+
5D	c306-GAL4/w; tsgal80/UAS-GFP-RNAi
5E	c306-GAL4/w; tsgal80/UAS-Sqh-RNAi
5F	c306-GAL4/w; tsgal80/UAS-α-Catenin-RNAi
5G	c306-GAL4/w; tsgal80/UAS-GFP-RNAi c306-GAL4/w; tsgal80/UAS-Sqh-RNAi c306-GAL4/w; tsgal80/UAS-α-Catenin-RNAi
6A-A"	c306-GAL4/w; tsgal80/+; UAS-LacZ.nls/+
6B-B"	c306-GAL4/w; tsgal80/UAS-Rap1N17; TM2/+
6C-C"	c306-GAL4, tsgal80/w; PT Fas III (GFP)/+; UAS-LacZ.nls/+
6D-D"	c306-GAL4, tsgal80/w; PT Fas III (GFP)/+; UAS-LacZ.nls/+
6E-E"	c306-GAL4, tsgal80/w; PT Fas III (GFP)/UAS-Rap1N17; TM2/+
6F-F"	c306-GAL4, tsgal80/w; PT Fas III (GFP)/UAS-Rap1N17; TM2/+

912

913

7A-A'	c306-GAL4/w; G13, L[2]/+; UAS-LacZ.nls/+
7B-B'	c306-GAL4/w; G13, L[2]/UAS-Rap1N17; TM2/+
7C	c306-GAL4/w; G13, L[2]/+; UAS-LacZ.nls/+ c306-GAL4/w; G13, L[2]/UAS-Rap1N17; TM2/+ c306-GAL4/w; G13, L[2]/+; UAS-mCherry-RNAi/+ c306-GAL4/w; G13, L[2]/+; UAS-Rap1-RNAi/+
7D-D'	c306-GAL4/w; tsgal80, UAS-Rap1N17/+; UAS-LacZ.nls/+
7E-E'	c306-GAL4/w; tsgal80, UAS-Rap1N17/UAS-p35.H
7F	c306-GAL4/w; tsgal80, UAS-Rap1N17/+; UAS-LacZ.nls/+ c306-GAL4/w; tsgal80, UAS-Rap1N17/UAS-p35.H
S1A-B	c306-GAL4/w; tsgal80/UAS-Rap1N17; TM2/+
S2A-A"	c306-GAL4/w; Sgh::GFP/+; UAS-LacZ.nls/+
S2B-B"	c306-GAL4/w; Sqh::GFP/UAS-Rap1N17; TM2/+
S2C	c306-GAL4/w; Sqh::GFP/+; UAS-LacZ.nls/+ c306-GAL4/w; Sqh::GFP/UAS-Rap1N17; TM2/+
S3A	c306-GAL4/w; tsgal80/+; UAS-LacZ.nls/+ c306-GAL4/w; tsgal80/UAS-Rap1N17; TM2/+ c306-GAL4/w; tsgal80/BL; UAS-Rap1V12/+
S3B	c306-GAL4/w; tsgal80, UAS-Rap1N17/+; UAS-LacZ.nls/+
S3C	c306-GAL4/w; tsgal80, UAS-Rap1N17/UAS-p35.H
S3D	c306-GAL4/w; tsgal80, UAS-Rap1N17/+; UAS-LacZ.nls/+ c306-GAL4/w; tsgal80, UAS-Rap1N17/UAS-p35.H
S4A	w; slbo-GAL4/UAS-LacZ.nls
S4B-B'	w; slbo-GAL4/UAS-LacZ.nls
S4C-C'	w; UAS-Rap1N17/+; slbo-GAL4/TM2
S4D	w; slbo-GAL4/UAS-LacZ.nls w; UAS-Rap1N17/+; slbo-GAL4/TM2
S5A-A"	c306-GAL4/w; 10XSTAT92E-GFP/+; UAS-LacZ.nls/+
S5B-B"	c306-GAL4/w; 10XSTAT92E-GFP/UAS-Rap1N17; TM2/+
S5C	c306-GAL4/w; 10XSTAT92E-GFP/+; UAS-LacZ.nls/+ c306-GAL4/w; 10XSTAT92E-GFP/UAS-Rap1N17; TM2/+

914
915

916 **Table 3. Antibodies used in this study.**

Antibody	Concentration	Source	Appears in Figures
Dcp-1 (Asp215)	(1:50-1:100)	Cell Signaling Technology	5, 6
DE-cadherin (DCAD2)	(1:10)	DSHB	1, 2, 3, 4, S1, S3
DIAP1	(1:100)	H. D. Ryoo	6
Eya (10H6)	(1:50-1:100)	DSHB	6
Fas3 (7G10)	(1:5-1:10)	DSHB	2, 4, 5, 7, S1, S3, S4, S5
GFP (12E6)	(1:10)	DSHB	1, S2
GFP (ab13970)	(1:100)	abcam	6, S5
LacZ (40-1a)	(1:10)	DSHB	1, S4
Lamin (ADL67.10)	(1:10)	DSHB	7, S4

Secondary antibodies used at a concentration of 1:400
Alexa Fluor Chicken 488 IgG H+L
Alexa Fluor Mouse 488 IgG H+L
Alexa Fluor Mouse 488 IgG1
Alexa Fluor Mouse 568 IgG H+L
Alexa Fluor Mouse 568 IgG2a
Alexa Fluor Rabbit 647 IgG H+L
Alexa Fluor Rat 488 IgG H+L
Alexa Fluor Rat 647 IgG H+L
DAPI (Millipore Sigma) was used at 0.05 µg/ml

917

918

919 **Table 4. Statistics in this study.**

Figure	Experimental Unit	Measurement	Experiments per Genotype (n)	Statistical Test	Significance
1G	Egg chamber	Anterior width	≥17	Unpaired two-tailed t test	**
2C	Polar cell	Aspect ratio	≥26	Unpaired two-tailed t test	ns, ****
3C	Egg chamber	Apical E-Cad Intensity	≥10	N/A	N/A
4E	Egg chamber	Anterior width	≥19	One-way ANOVA with Dunnett's Multiple Comparisons test	ns, **
5C	Ovariole	cDcp+ nuclei	≥29	One-way ANOVA with Dunnett's Multiple Comparisons test	ns, ****
5G	Ovariole	cDcp+ nuclei	≥20	One-way ANOVA with Dunnett's Multiple Comparisons test	ns, **
7C	Border cell clusters	Cells per cluster	≥26	Unpaired two-tailed t test	*, ****
7F	Border cell clusters	Cells per cluster	30	Unpaired two-tailed t test	***
S2C	Egg chamber	Apical Sqh Intensity	≥8	N/A	N/A
S3A	Egg chamber pole	Supernumerary polar cells	≥30	Fisher's exact test	ns, *
S3D	Polar cell	Aspect ratio	≥34	Unpaired two-tailed t test	ns
S4D	Border cell clusters	Cells per cluster	≥25	Unpaired two-tailed t test	****
S5C	Nucleus	Stat reporter intensity	≥12	Unpaired two-tailed t test	ns

920

921 Significance values: * P≤0.05, ** P≤0.01, ***P≤0.001, ****P<0.0001.